Estimating the seasonal impact of optically significant water constituents on surface heating rates in the Western Baltic Sea

Bronwyn E. Cahill[1,2], Piotr Kowalczuk[3], Lena Kritten[2], Ulf Gräwe[1], John Wilkin[4] and Jürgen Fischer[2]

[1]Physical Oceanography and Instrumentation, Leibniz Institute for Baltic Sea Research, Warnemünde 18119, Germany

[2]Institute of Meteorology, Free University Berlin, Berlin 12165, Germany

[3]Institute of Oceanology PAS, Powstańców Warszawy 55, 81-712 Sopot, Poland

[4]Department of Marine and Coastal Sciences, Rutgers University, New Brunswick, 08901 NJ, USA

Correspondence to: Bronwyn E. Cahill (bronwyn.cahill@io-warnemuende.de)

Abstract. Heating rates induced by optically significant water constituents (OSCs), e.g. phytoplankton and coloured dissolved organic matter (CDOM), contribute to the seasonal modulation of thermal energy fluxes across the ocean-atmosphere interface in coastal and regional shelf seas. This is investigated in the Western Baltic Sea, a marginal sea characterised by considerable inputs of freshwater carrying nutrients and CDOM, and complex bio-optical and hydrodynamic processes. Using a coupled bio-optical-ocean model (ROMS-Bio-Optic), the inherent optical properties of different OSCs are modelled under varying environmental conditions and the underwater light field is spectrally-resolved in a dynamic ocean. We estimate the relative contribution of these OSCs to the divergence of the heat flux and heating rates and find that while phytoplankton and CDOM both contribute to surface heating in summer, phytoplankton dominates the OSC contribution to heating in spring and summer, while CDOM dominates the OSC contribution to heating in summer and autumn. The study shows that seasonal and spatial changes in OSCs in the Western Baltic Sea have a small but noticeable impact on radiative heating in surface waters and consequences for the exchange of energy fluxes across the air-sea interface and the distribution of heat within the water column. In the Pomeranian Bight, where riverine influx of CDOM is strongest, water constituent-induced heating rates in surface waters in 2018 are estimated to be between 0.8 and 0.9 K m^{-1} d^{-1} in spring and summer, predominantly as a result of increased absorption by phytoplankton and CDOM. Further offshore, OSC-induced heating rates during the same periods are estimated to be between 0.4 and 0.8 K m^{-1} d^{-1}. Warmer surface waters are balanced by cooler subsurface waters. Surface heat fluxes (latent, sensible and longwave) respond to warmer sea surface temperatures with a small increase in heat loss to the atmosphere of 5 Wm^{-2} during the period April to September. We find relatively good agreement between our modelled water constituent absorption, and in situ and satellite observations. More rigorous co-located heating rate calculations using an atmosphere-ocean radiative transfer model provide evidence of the suitability of the ROMS-Bio-Optic model for estimating heating rates.

1 Introduction

Radiant energy fluxes impact biological production in the ocean and are modulated in turn as a result of biological production. This has fundamental consequences for upper ocean physics, surface nutrient supply, net primary and export

34 production and the exchange of soluble gases across the air-sea interface into the marine atmospheric boundary layer.

35 The contribution of optically significant water constituents (OSCs) to heating rates in the upper ocean is connected to

36 net primary and export production, through the direct effect of temperature on metabolic rates of marine plankton and

37 increased stratification and reduced vertical exchange of nutrients. This plays an important role in controlling the flow

38 of carbon and energy through pelagic systems (Wohlers et al., 2009; Taucher and Oschlies, 2011), in particular, the

39 partitioning between particulate and dissolved organic carbon, the transfer of primary produced organic matter to higher

40 trophic levels, the efficiency of the biological carbon pump and the exchange of CO_2 across the air-sea interface. Shelf

41 seas and coastal waters are characterised often by highly variable presence of inorganic suspended particulate matter

42 and coloured dissolved organic matter (CDOM). CDOM is the fraction of dissolved organic matter (DOM) that absorbs

43 light in natural waters in parts of the ultraviolet and visible spectral ranges (c. 200 - 550 nm). It is present throughout

44 the world oceans, both open and deep waters, and in coastal and shelf seas. It significantly contributes to the attenuation

45 of light in natural waters and thereby impacts ocean heat content, in particular in coastal and shelf seas (Soppa et al.,

46 2019; Gnanadesikan et al., 2019; Kim et al., 2015, 2016, 2018; Hill , 2008). In the Baltic Sea, CDOM is prevalent and

47 displays strong seasonal and spatial variability (Kowalczuk, 1999; Kowalczuk et al., 2006). Sources of CDOM and

48 changes to its composition through non-conservative processes are tightly coupled to the underwater light field. These

49 will vary with environmental conditions and phytoplankton community structure. Moreover, heterogeneity in

50 phytoplankton pigments and other water constituents will have implications for sub-mesoscale vertical mixing and

51 advective fluxes, and thus water temperature, density and the supply of nutrients to the surface. Understanding how the

52 variable presence of water constituents impacts energy fluxes in the upper ocean and across the air-sea interface, and the

53 accumulative effect on the upper ocean heat budget in shelf seas and coastal waters is of particular importance for our

54 capacity to adequately model regional ocean climate.

55 ~~A number of feedback mechanisms determine the biogeochemical dynamics in the upper ocean layer. Solar~~

56 ~~radiation penetrating the water column is scattered and absorbed by pure water, as well as by dissolved and particulate~~

57 ~~water constituents. Absorbed radiation is mostly transformed into heat and thus directly controls heating rates and~~

58 ~~subsequently impacts the vertical stratification of the euphotic layer. A portion of the light absorbed by autotrophic~~

59 ~~protists is used for photosynthesis and consequently contributes to biomass production. The vertical distribution of~~

60 ~~absorbing material may be altered significantly due to biogenic (and in coastal areas, non-biogenic) processes (e.g. by~~

61 ~~the development of a subsurface algae bloom) which in turn leads to a significant change of the depth range at which~~

62 ~~heating occurs (e.g. increased heating within the algae layer) and the availability of light (e.g. strongly reduced light~~

63 ~~availability below the algae layer).~~

64 ~~Biogeochemical dynamics are especially complex in shelf and coastal waters where organic and inorganic~~

65 ~~particulate matter as well as CDOM may be present in individually highly varying concentration ranges, e.g. caused by~~

66 ~~riverine inputs or sediment resuspension from the seafloor. For example, accounting for the highly variable light~~

67 ~~attenuation in turbid river plumes is critical if nearshore physics are to be resolved correctly (Cahill et al., 2008; Kim et~~

1.1 Ocean radiant heating and biological production

For studies of heat transfer modulated by biological production in the upper ocean, it is important to accurately prescribe the shortwave solar radiation in the upper water column. Downward solar radiation penetrating into the upper ocean can be partitioned into three spectral domains: Visible (UV/VIS): ~0.30 μm - ~0.75 μm; Near Infrared (NIR): ~0.75 μm - ~1.3 μm; Shortwave Infrared (SWIR): ~1.3 μm - ~3.5 μm. SWIR radiant energy plays an important role in the surface thermal structure of the water column, however, its attenuation can be considered as invariable to changes of water constituents (Morel and Antoine, 1994) as it is almost completely dominated by water absorption and is fully attenuated very close to the sea surface. NIR radiant energy penetrates a bit deeper into the ocean but is still almost entirely absorbed within the topmost one meter layer due to the still strong absorption of pure sea water at these wavelengths. In contrast to that, the (spectral) attenuation of UV/VIS radiant energy within the water body is strongly dependent on the presence of water constituents and may therefore vary considerably horizontally and vertically. More specifically, the variability of UV/VIS radiant energy in the water column is determined by absorption and scattering of optically significant water constituents, e.g.three substance classes: phytoplankton, detritus, CDOM and inorganic suspended sediment (Sathyendranath et al., 1989). Radiant energy within the visible range is also harvested by autotrophic protists for photosynthesis purposes. The properties of the individual constituents determine how they absorb and scatter light in different parts of the visible spectrum; CDOM preferentially absorbs light in the blue end of the spectrum while phytoplankton absorb light in the blue/green and red part of the spectrum, exactly how will depend on the pigment composition of the functional group (Figure 1).
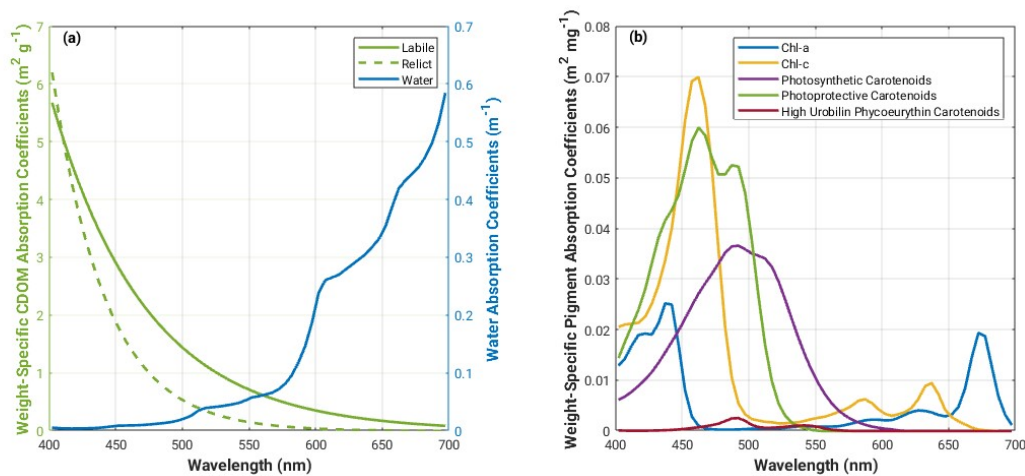

Figure 1: Spectral absorption coefficients for (a) water, relict and labile CDOM (Bissett et al., 1999b; Kowalczuk et al., 2005b) and (b) phytoplankton pigments (Bidigare et al., 1990) used in the Bio-Optic model.

A number of feedback mechanisms determine the biogeochemical dynamics in the upper ocean layer. ~~Solar radiation penetrating the water column is scattered and absorbed by pure water, as well as by dissolved and particulate water constituents.~~ Absorbed solar radiation is mostly transformed into heat and thus directly controls heating rates and subsequently impacts the vertical stratification of the euphotic layer. A portion of the light absorbed by autotrophic protists is used for photosynthesis and consequently contributes to biomass production. The vertical distribution of absorbing material may be altered significantly due to biogenic (and in coastal areas, non-biogenic) processes (e.g. by the development of a subsurface algae bloom or increased turbidity arising from sediment transport by river plumes) which in turn leads to a significant change of the depth range at which heating occurs (e.g. increased heating within the algae ~~layer~~or turbid layer) and the availability of light (e.g. strongly reduced light availability below the algae or turbid layer).

Biogeochemical dynamics are especially complex in shelf and coastal waters where organic and inorganic particulate matter as well as CDOM may be present in individually highly varying concentration ranges, e.g. caused by riverine inputs or sediment resuspension from the seafloor. For example, accounting for the highly variable light attenuation in turbid river plumes is critical if nearshore physics are to be resolved correctly (Cahill et al., 2008; Kim et al., 2020). Changes in surface temperature and buoyancy-driven circulation have important consequences for the development, transport and fate of phytoplankton biomass. The resulting carbon fluxes across the air-sea interface, exported to the benthos or advected off the shelf system are key to understanding the carbon budgets of shelf systems and the open ocean.

~~Biogeochemical dynamics in productive waters are characterized by the feedbacks between the absorption of light by dissolved and particulate material and the corresponding ocean radiant heating in the upper water column. This has been elegantly demonstrated for the open ocean where the upper ocean chlorophyll concentration regulates the radiant transmission and heating rates in the mixed layer depth (Lewis et al., 1990; Morel and Antoine, 1994; Ohlmann et al., 1996, 1998, 2000a, b; Murtugudde et al., 2002; Oschlies, 2004; Manizza et al., 2005, 2008). Enhanced near-surface stratification has a positive feedback on phytoplankton growth by restricting phytoplankton within shallower mixed layers with more available light, which in turn increases near surface local heating (Dickey and Falkowski, 2002). Ohlmann et al. (2000) demonstrated that an increase in chlorophyll concentration from 0.03 mg m^{-3} to 3 mg m^{-3} in the upper 10 m of the water column can decrease the solar flux in the waters below by as much as 35 Wm^{-2}. A 10 Wm^{-3} change in the solar radiation absorbed within a 10 m layer can represent a temperature change within that layer of more than 0.6°C month^{-1} (Simpson and Dickey, 1981). Löptien and Meier (2011) show that increased water turbidity affects the summer sea surface temperature trends in the Baltic Sea significantly.~~

1.2 Biogeochemical ocean models

A number of studies in productive open ocean waters elegantly demonstrate how upper ocean chlorophyll concentrations regulate radiant energy transmission and heating rates in the mixed layer (Simpson and Dickey, 1981; Lewis et al., 1990; Morel and Antoine, 1994; Ohlmann et al., 1996, 1998, 2000a, b; Dickey and Falkowski, 2002; Murtugudde et al., 2002; Oschlies, 2004; Manizza et al., 2005, 2008). Enhanced near-surface stratification can have a positive feedback on phytoplankton growth by restricting phytoplankton within shallower mixed layers with more available light, which in turn increases near surface local heating (Dickey and Falkowski, 2002). A 10 Wm^{-3} change in the solar radiation absorbed within a 10 m layer can represent a temperature change within that layer of more than 0.6°C month^{-1} (Simpson and Dickey, 1981). However, as light limitation is replaced by nutrient limitation, increased stratification will inhibit the exchange of deeper nutrient rich water with the surface and limit phytoplankton growth. Ohlmann et al. (2000) demonstrated that an increase in chlorophyll concentration from 0.03 mg m^{-3} to 3 mg m^{-3} in the upper 10 m of the water column can decrease the solar flux in the waters below by as much as 35 Wm^{-2}.

A few studies have tried to explore the full biophysical feedbacks using coupled physical-biological ocean models (Oschlies, 2004; Manizza et al., 2005; 2008) and fully coupled atmosphere-bio-physical ocean model (Jolliff and Smith, 2014; Wetzel et al., 2006). Notably, results from Oschlies (2004) include a net cooling of the North Atlantic by biota of about 1 Wm^{-2}, with enhanced upper ocean stratification in summer and deeper winter mixed layer depths (> 100 m) in parts of the subpolar gyre. Coastal upwelling and associated nutrient supply is reduced, especially in coastal upwelling regions of West Africa. Overall, there is a negative feedback of biotically induced radiative heating on chlorophyll-a concentrations, except in parts of the subpolar North Atlantic where intensification of the spring bloom results in increased annual mean chlorophyll-a concentrations. Wetzel et al. (2006) further highlighted the importance of marine biology on the radiative budget of the upper ocean, and found positive feedbacks with the climate system cause a global shift of the seasonal cycle, with the onset of spring occurring about two weeks earlier. Increased wind stress and changes in the shortwave radiation led to significant warming in the mid latitudes in summer and to seasonal modifications of the overall warming in the equatorial Pacific. Jolliff and Smith (2014) demonstrated a regional example of biological modulation of upper ocean physics in Monterey Bay, California and show how the spatiotemporal pattern of a phytoplankton bloom can persists because of enhanced thermal stratification promoting vertical stability and more efficient use of macronutrients. Furthermore, biothermal warming of surface waters modifies the local surface pressure gradient and modulates wind stress patterns.

More recent studies which investigate the role of OSCs and surface heating, highlight the role of CDOM in Arctic amplification (e.g. Soppa et al., 2019; Pefanis et al., 2020) and the impact of CDOM on the annual cycle of sea surface temperature in coastal and northern subpolar regions (Gnanadesikan et al., 2019; Kim et al., 2015; 2016; 2018). Soppa et al. (2019) found that a CDOM absorption at 443 nm of 1.77 m^{-1} contributed to an increased radiative heating of 0.6°C d^{-1} in the upper 2 m in the Laptev Sea shelf waters, implying increased sea ice melt rates and changes in the surface heat fluxes to the atmosphere. Pefanis et al. (2020) confirm that increases in CDOM in the Arctic amplify

surface warming by increasing surface temperatures in summer and decreasing sea-ice concentrations. They also show that summertime surface warming associated with increases in CDOM induces more heat loss to the atmosphere, primarily through latent and sensible heat fluxes. Gnanadesikan et al. (2019) demonstrate that the presence of CDOM leads to an increase in the amplitude of the seasonal cycle of SST over coastal and northern subpolar regions, with potential implications for extreme ocean temperatures. Importantly, they find the size and sign of the change in amplitude are controlled by the interplay between enhanced surface shortwave heating, shading and cooling of the subsurface and the extent to which these are connected by vertical mixing. They show that the interplay between heat term balances varies regionally. In the central Baltic Sea (58°N, 19.5°E), changes in the seasonal cycle of the heat budget are explained by a 1D balance between the penetration of shortwave radiation and vertical mixing (see Figure 3a in Gnanadesikan et al., 2019) with advective and diffusive terms being relatively small. In other regions around the world, the heat term balance is represented by a more complicated interplay between the penetration of shortwave radiation, vertical and horizontal mixing and advection (see Figure 3b, c, d in Gnanadesikan et al., 2019). Löptien and Meier (2011) show that increased water turbidity affects the summer sea surface temperature trends in the Baltic Sea significantly. While

Lastly, Skákala et al. (2022) demonstrate a significant impact of biogeochemistry on physics in the North West European Shelf, with the light attenuation by chlorophyll being responsible for a 1 °C warming in the upper 20 m of the ocean with comparable cooling taking place between 20 and 200 m. They also show that accounting for this water constituent-induced heating improves the timing of the simulated phytoplankton bloom in the region.

Despite these findings, coupled ecosystem-circulation models rarely share the same parameterization or source of radiative forcing to drive the hydrodynamics and fuel photosynthesis even though their requirements for information on light and heat overlap. This is in part due to the fact that historically, circulation and ecosystem models have evolved independently and it is only in the last 10 to 15 years that coupling between the two has made significant advances. It is typical that the ecosystem model is "plugged" into a circulation model and communication between the two is in one direction only: state variables (such as temperature) computed in the circulation model are communicated to the biological model at each time step, however, any change to the radiative fluxes as a consequence of biological activity is not necessarily accounted for or communicated back to the circulation model so that potentially available "information" related to heat transfer in the upper ocean and across the ocean-atmosphere interface is not being used.

Many parameterizations of the subsurface vertical distribution of shortwave solar radiation in ocean models have evolved over the last years (e.g. Paulson and Simpson, 1977; Zaneveld and Spinrad, 1980; Simpson and Dickey, 1981; Morel, 1988; Morel and Antoine, 1994; Ohlmann and Siegel, 2000; Manizza et al., 2008). For photosynthesis purposes, one of the more simple parameterizations of light attenuation is based on the surface photosynthetically available radiation (PAR) computed as a fraction of the net surface solar flux (typically 43%) and then attenuated through the water column as a function of chlorophyll concentration (e.g. Fasham et al., 1990; Fennel et al., 2006, 2008; Fennel and Wilkin, 2009). Zielinski et al. (2002) compare the effect of some different light parameterizations in biogeochemical

models on primary production and phytoplankton evolution in the subtropical North Atlantic and show that there can be significant changes in the vertical distribution of simulated phytoplankton, depending on how the underwater light field is treated.

The most common formulation of radiative forcing in bio-physical models is one-directional (i.e. assuming horizontal homogeneity) where radiative transfer is approximated by vertically attenuating the net surface shortwave radiation by an exponential function based on Beer-Lambert Law (Paulson and Simpson, 1977:

$$I_z = I_{IR} \cdot e^{-k_{IR}z} + I_{VIS} \cdot e^{-k_{VIS}z} \tag{1}$$

The total surface irradiance is split into two wavebands corresponding to infrared (IR) and visible (VIS), and the attenuation coefficients, k, for both the IR and VIS parts of the spectrum are prescribed according to different Jerlov (1976) water types. For photosynthesis purposes, one of the more simple parameterizations of light attenuation is based on the surface photosynthetically available radiation (PAR) computed as a fraction of the net surface solar flux (typically 43%) and then attenuated through the water column as a function of chlorophyll concentration (e.g. Fennel et al., 2006, 2008; Fennel and Wilkin, 2009). A further level of complexity may be introduced by splitting the visible portion of the light spectrum into two wavebands (red and blue/green) and computing the diffuse attenuation coefficients, k, for the two wavebands as a function of modelled chlorophyll concentration after Morel (1988) as described by Manizza et al. (2008):

$$I_z = I_{IR} \cdot e^{-k_{IR}z} + I_{RED(z-1)} \cdot e^{-k_{RED}\Delta z} + I_{BLUE(z-1)} \cdot e^{-k_{BLUE}\Delta z} \tag{2}$$

~~This c~~Chlorophyll-based approach~~es to underwater light attenuation is~~ ~~are~~ reasonably accurate for the open ocean where phytoplankton dominates the inherent optical properties of the water constituents (Morel and Prieur, 1977); however, ~~it is~~they are inadequate in shelf and coastal oceans as ~~it~~ they neglect~~s~~ important contributions from CDOM, detritus and suspended sediments. ~~More recently,~~ Neumann et al. (2015) show that, in the Baltic Sea, including more water constituents in the estimation of light attenuation in their model yields a more realistic representation of the light climate, and improved estimates of primary productivity, Secchi disk depth and oxygen concentrations. They estimate ~~K(PAR)~~light attenuation by explicitly accounting for modelled phytoplankton biomass, detritus, dissolved organic matter due to metabolism and degradation processes, and parameterizing CDOM as a function of salinity~~., as follows:~~

$$K_{PAR} = k_w + k_c Chl + k_{det} DET + k_{don} DON + k_{CDOM}(S) \tag{3}$$

226

More recently, Neumann et al. (2021) explicitly consider light absorption due to terrestrial CDOM in their ecosystem model of the Baltic Sea, using earth observation CDOM absorption data from Sentinel-2 MSI as a proxy for terrestrial sources of CDOM. They show a significant improvement in CDOM estimates in particular in the northern parts of the Baltic Sea where the impacts of terrestrial CDOM are large.

Including directional and spectral light in coupled biogeochemical-circulation-radiative models has been shown to be important for ocean biology, especially for studies of community structure and succession (Gregg and Rousseaux, 2016). It is also important for regional studies which examine the role of other optical constituents such as CDOM and detritus in carbon cycling (Bissett et al., 1999a,b).

A few studies have tried to explore the full biophysical feedbacks using coupled physical-biological ocean models (Oschlies, 2004; Manizza et al., 2005; 2008) and fully coupled atmosphere-bio-physical ocean model (Jolliff and Smith, 2014; Wetzel et al., 2006). Notably, results from Oschlies (2004) include a net cooling of the North Atlantic by biota of about 1 Wm^{-2}, with enhanced upper ocean stratification in summer and deeper winter mixed layer depths (> 100 m) in parts of the subpolar gyre. Coastal upwelling and associated nutrient supply is reduced, especially in coastal upwelling regions of West Africa. Overall, there is a negative feedback of biotically induced radiative heating on chlorophyll-a concentrations, except in parts of the subpolar North Atlantic where intensification of the spring bloom results in increased annual mean chlorophyll-a concentrations. Wetzel et al. (2006) further highlighted the importance of marine biology on the radiative budget of the upper ocean, and found positive feedbacks with the climate system cause a global shift of the seasonal cycle, with the onset of spring occurring about two weeks earlier. Increased wind stress and changes in the shortwave radiation led to significant warming in the mid latitudes in summer and to seasonal modifications of the overall warming in the equatorial Pacific. Jolliff and Smith (2014) demonstrated a regional example of biological modulation of upper ocean physics in Monterey Bay, California and show how the spatiotemporal pattern of a phytoplankton bloom can persists because of enhanced thermal stratification promoting vertical stability and more efficient use of macronutrients. Furthermore, biothermal warming of surface waters modifies the local surface pressure gradient and modulates wind stress patterns.

More recent studies which investigate the role of OSCs and surface heating, highlight the role of CDOM in Arctic amplification (e.g. Soppa et al., 2019; Pefanis et al., 2020) and the impact of CDOM on the annual cycle of sea surface temperature in coastal and northern subpolar regions (Gnanadesikan et al., 2019; Kim et al., 2015; 2016; 2018). Soppa et al. (2019) found that a CDOM absorption at 443 nm of 1.77 m^{-1} contributed to an increased radiative heating

of 0.6°C d⁻¹ in the upper 2 m in the Laptev Sea shelf waters, implying increased sea ice melt rates and changes in the surface heat fluxes to the atmosphere. Pefanis et al. (2020) confirm that increases in CDOM in the Arctic amplify surface warming by increasing surface temperatures in summer and decreasing sea-ice concentrations. They also show that summertime surface warming associated with increases in CDOM induces more heat loss to the atmosphere, primarily through latent and sensible heat fluxes. Gnanadesikan et al. (2019) demonstrate that the presence of CDOM leads to an increase in the amplitude of the seasonal cycle of SST over coastal and northern subpolar regions, with potential implications for extreme ocean temperatures. Importantly, they find the size and sign of the change in amplitude are controlled by the interplay between enhanced surface shortwave heating, shading and cooling of the subsurface and the extent to which these are connected by vertical mixing. They show that the interplay between heat term balances varies regionally. In the central Baltic Sea (58°N, 19.5°E), changes in the seasonal cycle of the heat budget are explained by a 1D balance between the penetration of shortwave radiation and vertical mixing (see Figure 3a in Gnanadesikan et al., 2019) with advective and diffusive terms being relatively small. In other regions around the world, the heat term balance is represented by a more complicated interplay between the penetration of shortwave radiation, vertical and horizontal mixing and advection (see Figure 3b, c, d in Gnanadesikan et al., 2019).

Lastly, Skákala et al. (2022) demonstrate a significant impact of biogeochemistry on physics in the North West European Shelf, with the light attenuation by chlorophyll being responsible for a 1 °C warming in the upper 20 m of the ocean with comparable cooling taking place between 20 and 200 m. They also show that accounting for this water constituent-induced heating improves the timing of the simulated phytoplankton bloom in the region.

1.3 Estimating the impact of optically significant water constituents on surface heating in the Western Baltic Sea

In this work, we use a spectrally-resolved underwater light field to examine explore the relationship between OSCs, in particular, CDOM, phytoplankton and detritus, and heating rates in the Western Baltic Sea. High concentrations of CDOM optically distinguish the Baltic Sea from other coastal seas (Simis et al., 2017), making it an interesting study site for this application. CDOM also exhibits strong seasonal and spatial variability in the region which is dependent on sources of CDOM and physics, e.g. periods of intensive mixing and high riverine discharge versus periods of thermal stratification, reduced riverine discharge, enhanced biological production and production of CDOM (Kowalczuk, 1999; Kowalczuk et al, 2005a). In this study, wWe examine precisely this interplay between physics and OSCs using an integrated analysis framework. This consists of a coupled bio-optical ocean model which incorporates the optical properties of key water constituents and explicitly resolves sources of both terrestrial and authochthonous CDOM as a state variable in a 4D ocean state. We model the inherent optical properties of different water constituents under varying environmental conditions and spectrally resolve the underwater light field in a dynamic ocean. From this, we estimate the contribution of key water constituents to surface heating rates and feedbacks with the marine atmospheric boundary layer heat fluxes. We evaluate our estimates of surface heating rates using an ocean atmosphere radiative transfer model andmodelled inherent and apparent optical properties with measurements from in situ and

293 ~~remote sensing~~satellite observations and our estimates of surface heating rates using an ocean-atmosphere radiative
294 transfer model which accounts for both the directionality and spectral dependence of the underwater light field.

2 Methods

2.1 Study site

Kowalczuk et al. (2006) have shown that there are three pools of CDOM in the waters of the Southern Baltic Sea: a riverine pool, an aged marine pool and a pool primarily produced in offshore waters. They explored the seasonal dependence between the light absorption coefficient of CDOM at 375 nm, aCDOM(375), and salinity and chlorophyll-a concentrations in the Southern Baltic Sea and found a seasonal dependence between physical processes and the source of CDOM. In March, April and November, months of intensive mixing and high riverine discharge, most of the variability in aCDOM(375) values could be explained by dilution of terrestrially derived CDOM alone. In February, May and September, months of thermal stratification, reduced riverine discharge and enhanced biological activity, autochthonous production of CDOM was found to be a significant source of CDOM in the Southern Baltic Sea. Changes in the values of spectral slope coefficients are regarded as an indicator of compositional changes in CDOM. These changes can be a result of either conservative mixing processes, i.e. mixing, or non-conservative processes, e.g. production, degradation or flocculation (Kowalczuk et al., 2006).
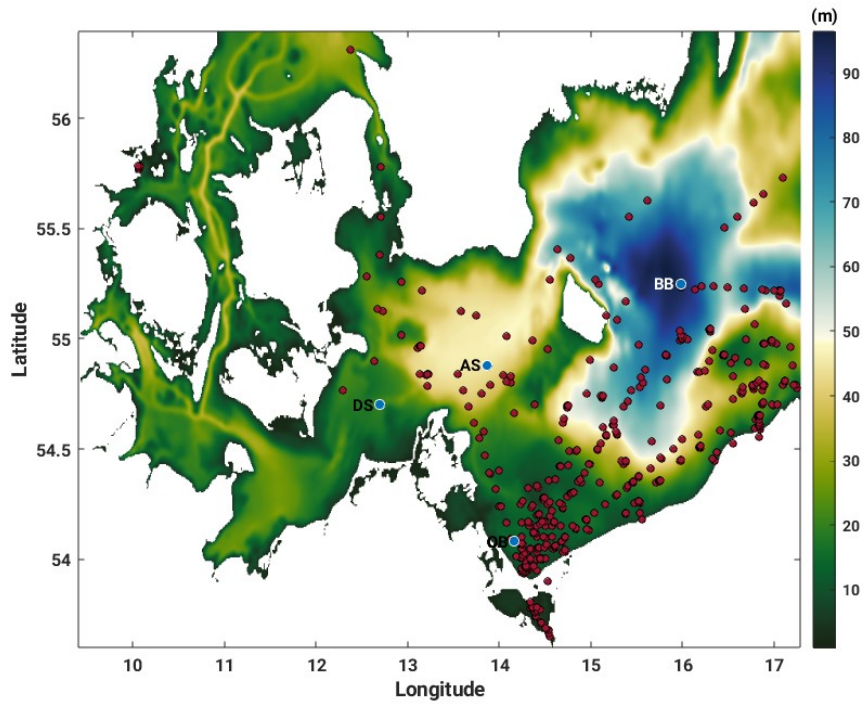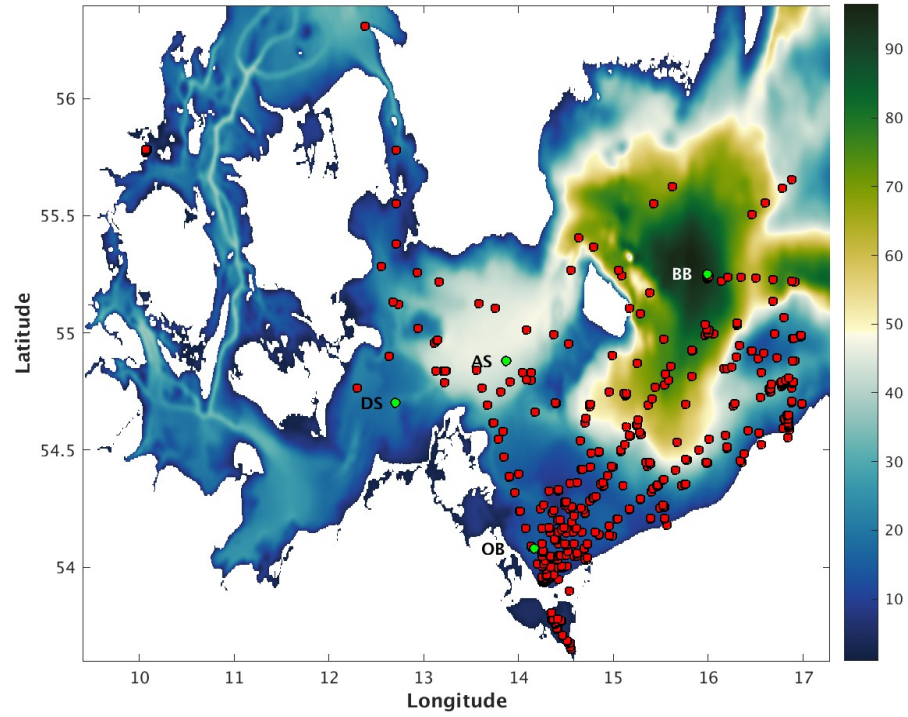
309

310

311

312 Figure 12: Western Baltic Sea model domain bathymetry (m) with location of model output analysis stations, Darß Sill

313 (DS), Arkona Sea (AS), Oder Bank (OB) and Bornholm Basin (BB) (green blue dots) and in situ CDOM and NAP

314 (non-algal particle) absorption measurements from the Institute of Oceanology of the Polish Academy of Sciences,

315 IOPAN (red dots).

Our study site in the Western Baltic Sea (Figure 2~~1~~) includes the Bornholm Basin, where we expect the seasonal cycle to be explained by a 1D balance between the penetration of shortwave radiation and vertical mixing (Gnanadesikan et al., 2019), and the Darß Sill, Arkona Sea and Oder Bank, where advection and diffusion will also contribute to the seasonal heat balance, making for an interesting contrast between local regimes. At the Bornholm Basin, we expect to find marine CDOM, at the Darß Sill and Arkona Sea, we expect to find a mixture of riverine and marine CDOM, depending on the season, while at the Oder Bank, we expect the CDOM pool to be dominated by riverine sources from multiple inlets and rivers connecting the Oder River outlet through Szczecin Lagoon with the Greifswalder Bodden and the coastal Baltic Sea (Kowalczuk et al., 1999).

2.2 Theory

Light penetrating a water body can be described as consisting of three streams (Aas, 1987; Ackleson et al., 1994; Gregg, 2002 and Dutkiewicz et al., 2015). These are the downward direct irradiance, E_{dir}, the downward diffuse irradiance, E_{diff} and the upward diffuse irradiance, E_u. $E_{dir} + E_{diff}$ is commonly referred to as downward irradiance, E_d. For studies of heat transfer and photosynthesis, we need to know the scalar irradiance, E_0, which describes the light field integrated over a sphere, and is thus independent of direction. All of these irradiance quantities (E_{dir}, E_{diff}, E_u and E_0) are a function of wavelength and depth.

Following Morel (1988), the rate of radiant energy converted into heat can be estimated as follows:

$$\frac{dT}{dt} = \frac{-d(E_d - E_u)}{dz} \frac{1}{\rho C_p} \tag{4}$$

where the first term on the right hand side is the heat flux, E_d and E_u are the downward and upward irradiances, respectively, ρ is the in situ density and C_p is the specific heat capacity of water. In a horizontally homogeneous water body, the divergence of the radiative flux can be approximated as follows (Morel, 1988):

$$\frac{d(E_d - E_u)}{dz} \cong -aE_0 \approx K_d E_d \tag{5}$$

where a is the local absorption coefficient, E_0 is the scalar irradiance at the depth in question and K_d is the downward diffuse attenuation coefficient for downwelling irradiance. These quantities are all dependent on depth, concentrations of OSCs (e.g. phytoplankton pigments, CDOM, detritus) and wavelength. Thus,

$$\frac{dT}{dt} = \frac{-\int_{400}^{700}[E_d(\lambda,z).K_d(\lambda,z)]d\lambda}{\rho C_p} \tag{6}$$

K_d varies with both absorption, a, and scattering b, as well as with the angular distribution of the incoming light field. It can be calculated from E_d, as follows (Gordon et al., 1980):

$$K_d = \frac{-d\ln E_d(\lambda,z)}{dz} = \frac{-1}{E_d(\lambda,z)}\frac{dE_d(\lambda,z)}{dz} \tag{7}$$

Biogeochemical-optical relationships vary significantly over different regions and/or seasons, therefore, regional and temporal relationships have been adopted to cope with such variations when information concerning the directionality of the underwater light field is limited. For example, in open ocean waters, where attenuation of underwater light is primarily a function of chlorophyll concentration, Sathyendranath and Platt (1988) parameterize K_d, as follows:

$$K_d = \frac{a+b}{\mu_0} \tag{8}$$

where a is the absorption and b is the total scattering (forward and backscatter) of OSCs, while μ_0 is the average cosine, which tells you how much the light field differs from isotropic conditions.

In more complex coastal waters, Lee et al. (2005) have derived an empirical algorithm to parameterize K_d, as follows:

$$K_d = (1 + 0.005\theta)a(\lambda,z) + 4.18 \tag{9}$$

where θ is the solar zenith angle in degrees and b_b is the backscatter coefficient.

If the absorption and scattering properties of different water constituents are known, K_d can be estimated using Eq. (8) or Eq. (9) and E_d can then be calculated using Eq. (10).

$$E_d = E_d(0)e^{-K_d z} \tag{10}$$

Thus, the heat balance relationship described in Eq. (6), can be used to estimate heating rates.

2.23 Model system

The coupled modelling system has two components: the Regional Ocean Modelling System, ROMS, which drives the physics and the advection and diffusion of tracers, and Ecosim/Bio-Optic which drives the ecosystem and underwater light field. These components interact as shown in Figure 3 and are described in more detail below.
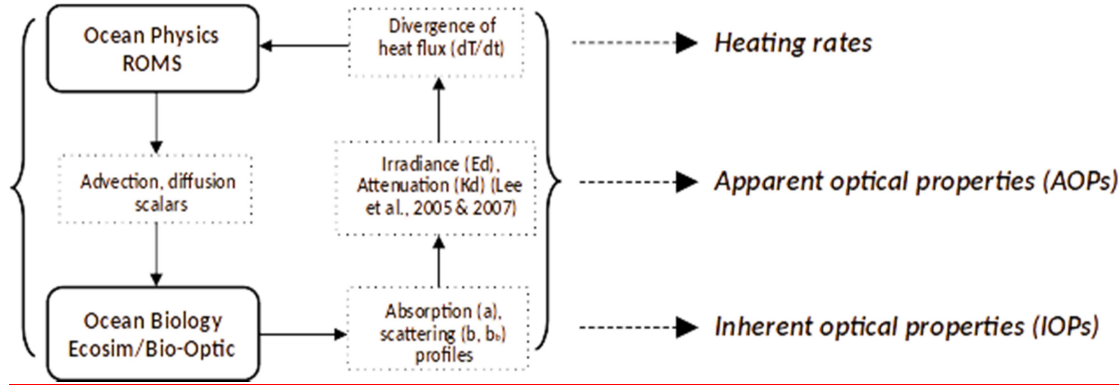

Figure 3: Model system components and how they interact

Light penetrating a water body can be described as consisting of three streams (Aas, 1987; Ackleson et al., 1994; Gregg, 2002 and Dutkiewicz et al., 2015). These are the downward direct irradiance, E_{dir}, the downward diffuse irradiance, E_{diff} and the upward diffuse irradiance, E_u. E_{dir} + E_{diff} is commonly referred to as downward irradiance, E_d. For studies of heat transfer and photosynthesis, we need to know the scalar irradiance, E_0 which describes the light field integrated over a sphere, and is thus independent of direction. All of these irradiance quantities (E_{dir}, E_{diff}, E_u and E_0) are a function of wavelength and depth.

Following Morel (1988), the rate of radiant energy converted into heat can be estimated as follows:

$$\frac{dT}{dt} = -\frac{d(E_d - E_u)}{dz}\frac{1}{\rho C_p} \tag{1}$$

where the first term on the right hand side is the heat flux, E_d and E_u are the downward and upward irradiances, respectively, ρ is the in situ density and C_p is the specific heat capacity of water. In a horizontally homogeneous water body, the divergence of the radiative flux can be approximated as follows (Morel, 1988):

$$\frac{d(E_d - E_u)}{dz} \cong -aE_0 \approx K_d E_d \tag{2}$$

where a is the local absorption coefficient, E_0 is the scalar irradiance at the depth in question and K_d is the downward diffuse attenuation coefficient for downwelling irradiance. These quantities are all dependent on depth, concentrations of OSCs (e.g. phytoplankton pigments, CDOM, detritus) and wavelength. Thus,

$$\frac{dT}{dt} = -\frac{\int_{400}^{700} \left[E_d\left(\lambda, z\right) K_d\left(\lambda, z\right) \right] d\lambda}{\rho C_p} \tag{3}$$

K_d varies with both absorption, a, and scattering b, as well as with the angular distribution of the incoming light field. It can be calculated from E_d, as follows (Gordon et al., 1980):

$$K_d = \frac{-d \ln E_d\left(\lambda, z\right)}{dz} = \frac{-1}{E_d\left(\lambda, z\right)} \frac{dE_d\left(\lambda, z\right)}{dz} \tag{4}$$

Biogeochemical-optical relationships vary significantly over different regions and/or seasons, therefore, regional and temporal relationships have been adopted to cope with such variations when information concerning the directionality of the underwater light field is limited. For example, in open ocean waters, where attenuation of underwater light is primarily a function of chlorophyll concentration, Sathyendranath and Platt (1988) parameterize K_d, as follows:

$$K_d = \frac{a+b}{\mu_0} \tag{5}$$

where a is the absorption and b is the total scattering (forward and backscatter) of OSCs, while μ_0 is the average cosine, which tells you how much the light field differs from isotropic conditions.

In more complex coastal waters, Lee et al. (2005) have derived an empirical algorithm to parameterize K_d, as follows:

$$K_d = \left(1 + 0.005\theta\right) a\left(\lambda, z\right) + 4.18\left(1 - 0.52 e^{-10.8 a\left(\lambda, z\right)} b_b\left(\lambda, z\right)\right) \tag{6}$$

where θ is the solar zenith angle in degrees and b_b is the backscatter coefficient.

If the absorption and scattering properties of different water constituents are known, K_d can be estimated using Eq. (5) or Eq. (6) and E_d can then be calculated using Eq. (7).

$$E_d = E_d\left(0\right) e^{-K_d z} \tag{7}$$

Thus, the heat balance relationship described in Eq. (3), can be used to estimate heating rates.

2.3 2.1 Regional Ocean Modelling System, ROMS and Ecosim/Bio-Optic

The ocean model component, ROMS, is widely used for shelf circulation (e.g. Haidvogel et al., 2008, Wilkin et al., 2011) and coupled physical-biological applications (e.g. Cahill et al., 2008; 2016, Fennel et al., 2006; 2008; 2013, Fennel and Wilkin, 2009). The ROMS computational kernel (Shchepetkin and McWilliams, 2005) produces accurate evolution of tracer fields, which is a particularly attractive feature for biogeochemical modelling because it facilitates

the correct interaction among tracers and accounting of total nutrient and carbon budgets. ~~Within~~ ROMS ~~, we have incorporated a novel spectrally-resolved bio-optical module, herein called Bio-Optic.~~

~~BioOptic is an adaptation of~~ is coupled to Ecosim, the carbon-based, ecological/optical modelling system ~~Ecosim~~ (Bissett et al., 1999a, b) which was developed for simulations of carbon cycling and biological productivity~~. It~~ Ecosim simulates up to four phytoplankton functional groups each with a characteristic pigment suite which varies with the group carbon-to-chlorophyll-a ratio, C:Chla. The properties of each functional group evolve over time as a function of light and nutrient conditions (i.e. NO_3, NH_4, PO_4, SiO and FeO). Marine and riverine sources of dissolved organic carbon (DOC and CDOC) are accounted for and explicitly resolved into labile (e.g. available for biological and photo-degradation) and relict (e.g. available for photo-degradation) forms. Dissolved inorganic carbon is also accounted for. Riverine sources of carbon and nutrients are introduced via point sources. The underwater light field is spectrally-resolved between 400 and 700 nm, which allows for differential growth of different phytoplankton groups that have unique pigment complements. The interaction between Ecosim's components describe autotrophic growth of and competition between phytoplankton groups, differential carbon and nitrogen cycling, nitrogen fixation and grazing. Coupled ROMS-Ecosim applications include a deployment in the New York / New Jersey sea bight which demonstrates how turbid buoyant plumes originating from the Hudson River feedback on near-shore biogeochemistry and physics (Cahill et al., 2008).

Ecosim contains a daylight module which is central to this work. Light energy just beneath the sea surface is calculated using a derivative of the RADTRAN code described in Gregg and Carder (1990) as a function of the model's meteorological forcing (i.e. wind speed, relative humidity, air temperature and pressure), and cloud cover, atmospheric gases (i.e. water vapour, ozone, oxygen), marine aerosols and the surface roughness and reflectance at the ocean-atmosphere interface. A constant fraction of 0.3 cloud cover is assumed for clouds, while 1.5 cm precipitable water is assumed for water vapour. The underlying algorithms used to compute ozone, water vapour and oxygen absorption coefficients are described in detail in Gregg and Carder (1990). Marine aerosols are computed according to the simplified version of the Navy marine aerosol model, also described in detail in Gregg and Carder (1990). The surface solar downwelling spectral irradiance, $E_d(\lambda,0-)$ (which is the sum of the direct and diffuse irradiance) and the average cosine zenith angle, $\mu_0(\lambda,0-)$ are provided at 5 nm wavelength intervals between 400 and 700 nm and are used as inputs to Ecosim's daylight module.

The spectrally-resolved downward light stream, $E_d(\lambda,z)$~~, which~~ is calculated according to Eq. (10)~~, incorporates both direct and diffuse components of the light field~~ and is attenuated by absorption, a, and scattering, b (forward, b and backward, b_b) of ~~phytoplankton, detritus and CDOM~~ the OSCs. Phytoplankton and detritus both absorb and scatter light. Phytoplankton absorption is calculated for the four functional groups as a function of biomass, weight-specific pigment absorption coefficients (Figure 1b, Bidigare et al., 1990) and packaging effect (Bissett et al., 1999b; Kirk, 2011). Detrital absorption is calculated as an exponential function of wavelength (Gallegos et al., 2011). Phytoplankton and detrital scattering and backscattering are accounted for as total particulate scattering and backscattering according to

16

Morel (1991) and Morel (1988), respectively (see Equations 16 and 17 in Bissett et al., 1999b). CDOM only absorbs light and is calculated as a function of CDOM concentration and the weight-specific absorption coefficients adapted from Kowalczuk et al. (2005b) (Figure 1a). The average cosine is modified with depth as a function of absorption and backscattering. This is simplified as a linear function of the optical depth between two levels (see Equation 22 in Bissett et al., 1999b). , and tThe total scalar irradiance, $E_0(\lambda,z)$, which is the light available to phytoplankton, is calculated following Eq. (5) after Morel (1988). BioOptic builds on Ecosim's functionality as follows. T

Bio-Optic is a new option within Ecosim's daylight module which adds some diagnostics and functionality. These are:

- downwelling irradiance attenuation coefficient, K_d, is calculated following Eq. (9) after Lee et al. (2005). hethe explicit output of inherent optical property diagnostics inherent optical properties (absorption, scatter and backscatter) of each of the OSCs (i.e. phytoplankton, detritus and CDOM) are explicitly resolved and their individual contribution to tapparent optical property diagnostics (he downward attenuation and, downward and scalar irradiance fields, is calculated. The surface solar downwelling spectral irradiance, $E_d(\lambda,0-)$ and the average cosine zenith angle, $\mu_0(\lambda,0-)$).

- an option to calculate a downwelling irradiance attenuation coefficient, K_d, which accounts for some of the optical complexity found in coastal waters, according to Lee et al. (2005).

- an option to couple the bio-optically calculated downward irradiance term back into the hydrodynamic solution. , just beneath the sea surface, are calculated according to Gregg and Carder (1990). This includes the impact of clouds, water vapour and aerosols in the atmosphere and the surface roughness and reflectance at the ocean-atmosphere interface. Spectral irradiances between 400 and 700 nm are provided at 5 nm intervals. The downwelling irradiance attenuation coefficient, K_d, is calculated following Eq. (9) after Lee et al. (2005).

The spectrally-resolved downward light stream, $E_d(\lambda,z)$, which is calculated according to Eq. (10), incorporates both direct and diffuse components of the light field and is attenuated by absorption, a, and scattering, b (forward, b and backward, b_b) of phytoplankton, detritus and CDOM. The average cosine is modified with depth as a function of absorption and backscattering, and the total scalar irradiance, $E_0(\lambda,z)$, which is the light available to phytoplankton, is calculated following Eq. (5) after Morel (1988). Bio-Optic is activated as an option within Ecosim during compilation.

Light penetrating a water body can be described as consisting of three streams (Aas, 1987; Ackleson et al., 1994; Gregg, 2002 and Dutkiewicz et al., 2015). These are the downward direct irradiance, E_{dir}, the downward diffuse irradiance, E_{diff} and the upward diffuse irradiance, E_u. $E_{dir} + E_{diff}$ is commonly referred to as downward irradiance, E_d. For studies of heat transfer and photosynthesis, we need to know the scalar irradiance, E_0 which describes the light field integrated over a sphere, and is thus independent of direction. All of these irradiance quantities (E_{dir}, E_{diff}, E_u and E_0) are a function of wavelength and depth.

Following Morel (1988), the rate of radiant energy converted into heat can be estimated as follows:

$$\frac{dT}{dt} = \frac{-d(E_d - E_u)}{dz} \cdot \frac{1}{\rho C_p} \qquad (4)$$

where the first term on the right hand side is the heat flux, E_d and E_u are the downward and upward irradiances, respectively, ρ is the in situ density and C_p is the specific heat capacity of water. In a horizontally homogeneous water body, the divergence of the radiative flux can be approximated as follows (Morel, 1988):

$$\frac{d(E_d - E_u)}{dz} \cong -aE_0 \approx K_d E_d \qquad (5)$$

where a is the local absorption coefficient, E_0 is the scalar irradiance at the depth in question and K_d is the downward diffuse attenuation coefficient for downwelling irradiance. These quantities are all dependent on depth, concentrations of OSCs (e.g. phytoplankton pigments, CDOM, detritus) and wavelength. Thus,

$$\frac{dT}{dt} = \frac{-\int_{400}^{700}[E_d(\lambda,z).K_d(\lambda,z)]d\lambda}{\rho C_p} \qquad (6)$$

K_d varies with both absorption, a, and scattering b, as well as with the angular distribution of the incoming light field. It can be calculated from E_d, as follows (Gordon et al., 1980):

$$K_d = \frac{-d\ln E_d(\lambda,z)}{dz} = \frac{-1}{E_d(\lambda,z)} \frac{dE_d(\lambda,z)}{dz}$$
$$(7)$$

Biogeochemical-optical relationships vary significantly over different regions and/or seasons, therefore, regional and temporal relationships have been adopted to cope with such variations when information concerning the directionality of the underwater light field is limited. For example, in open ocean waters, where attenuation of underwater light is primarily a function of chlorophyll concentration, Sathyendranath and Platt (1988) parameterize K_d, as follows:

$$K_d = \frac{a+b}{\mu_0} \qquad (8)$$

where a is the absorption and b is the total scattering (forward and backscatter) of OSCs, while μ_0 is the average cosine, which tells you how much the light field differs from isotropic conditions.

In more complex coastal waters, Lee et al. (2005) have derived an empirical algorithm to parameterize K_d, as follows:

$$K_d = (1 + 0.005\theta)a(\lambda, z) + 4.18 \tag{9}$$

where θ is the solar zenith angle in degrees and b_b is the backscatter coefficient.

If the absorption and scattering properties of different water constituents are known, K_d can be estimated using Eq. (8) or Eq. (9) and E_d can then be calculated using Eq. (10).

$$E_d = E_d(0)e^{-K_d z} \tag{10}$$

Thus, the heat balance relationship described in Eq. (6), can be used to estimate heating rates.

The explicit calculation of in-water spectrally-resolved absorption, scattering and backscattering coefficients, average cosine, downwelling irradiance attenuation coefficient, K_d, in addition to the scalar, E_0, and downward, E_d, irradiance fields, has important implications. The spectrally-resolved underwater light field drives the evolution of OSCs in the ecosystem model, while the OSCs in turn determine the evolution of the light field in each layer by absorption and scattering of the light. This means that the OSCs' contribution to the divergence of the heat flux (Morel, 1988) can be accounted for within the full hydrodynamic solution. Furthermore, water constituent-induced heating rates can be assessed and their impact on the ocean sea surface temperature is can be communicated to the bulk flux formulation of the atmosphere in the modelling system.

While this still represents a very simplified treatment of radiative transfer within the water column, it does permit a direct evaluation of the optical terms and heating rates with those derived from a full solution of the radiative transfer equations and provides a means to improving the parameterization of water constituent-based heat flux algorithms in ocean models. For this purpose, we use the vector radiative transfer model, MOMO (described below) to evaluate the more approximate solution provided by ROMS-Bio-Optic.

2.3 2.2 Vector radiative transfer model, MOMO

A more rigorous treatment of the vertical structure of the light field is provided by atmosphere-ocean radiative transfer models, such as MOMO (Fell and Fischer, 2001), which simulate the light field in the stratified atmosphere-ocean system for the VIS and NIR spectral ranges. MOMO uses the matrix operator method to calculate zenithally and azimuthally resolved light fields for different types and concentrations of optically active components in the ocean and atmosphere, thus, the full directionality of the light field is accounted for. The main advantage of the matrix-operator method is its efficiency in simulating light propagation in optically dense media. It is therefore particularly suited for the use in the development of remote sensing algorithms for the retrieval of water constituents. It is most recently described in Hollstein and Fischer (2012) and is based on previous work by Fischer and Grassl (1984) and Fell and Fischer (2001). It has been successfully applied to remote sensing of lakes (Heege and Fischer, 2004), analysis of hyper-

spectral, ocean colour data to derive surface fluorescence signals (Guanter et al., 2010), analysis of ocean color data from MERIS measurements (Zhang et al., 2003) and a new retrieval of sun-induced chlorophyll fluorescence in water from ocean colour measurements (Kritten et al., 2020). For our purposes, the most pertinent elements of MOMO include the calculation of the spectrally-resolved downward surface irradiance for the VIS and NIR ranges, the direct and diffuse downwelling and the diffuse upwelling components of the underwater light field.

2.4 3 Experimental setup

The ROMS Ecosim/Bio-Optic modelling system was configured for the Western Baltic Sea (Figure 3?) as described in Table 1 with . The model domain has a horizontal resolution of ~ 1.8km with (285 x 169 grid points in the horizontal) , and 30 sigma levels in the vertical. , aA bulk flux atmosphere was forced with DWD-ICON output (Zängl et al., 2015) and river forcing including runoff and biogeochemistry was derived from HELCOM PLC (Pollution Load Compilation) data (Neumann, pers. comm). Open boundaries to the north and east were forced with output from GETM physics (Gräwe et al., 2015a, b) using a combination of Chapman / Flather conditions for u and v velocities and transports, and Radiation + Nudging for temperature and salinity. This 3D setup is based on an existing GETM physics setup which has been previously evaluated and published (Gräwe et al., 2015a,b). It captures the annual cycle of temperature and salinity in the Western Baltic Sea and episodic inflows of saline, oxygen-rich North Sea water which control the salinity content and stratification in the Baltic Sea and are important for ventilating the deeper basins of the Baltic Sea (Omstedt et al., 2004; Meier, 2007).

Ecosim was configured with four phytoplankton functional groups representative of small and large diatoms, large dinoflagellates and cyanobacteria. We focus our evaluation on the modelled inherent optical properties of the water constituents using observations from Kowalczuk et al. (2005a,b) and Meler et al. (2016a,b).

We performed two experiments, as follows:

1. 3D Western Baltic Sea, feedback of constituent-induced heating into hydrodynamic solution (herein referred to as "biofeed")
2. 3D Western Baltic Sea, no feedback of constituent-induced heating into hydrodynamic solution (herein referred to as "nobiofeed")

The simulation period for both experiments was 2018.

Table 1: Model configuration

Model Configuration	
Components	3D Western Baltic Sea
Model Grid	285 x 169 (1nm), 30 sigma levels
Simulation Period	2018

~~Boundary Conditions~~	~~Chapman for zeta, Flather for ubar and vbar; Radiation + Nudging for temperature and salinity~~
~~Bulk Flux Atmosphere~~	~~DWD ICON 3 hourly~~
~~River Forcing~~	~~HELCOM PLC (Pollution Load Compilation), Neumann (pers. comm.)~~
~~Initial Condition~~	~~GETM / ERGOM~~
~~Time Step~~	~~DT = 30s; NDTFAST = 20s~~
~~Evaluation~~	~~Water constituent absorption:~~
	~~• Kolwaczuk et al, 2005; Meler et al., 2016; MERIS Climatology~~ ~~Water constituent induced heating rates:~~
	~~• Comparable MOMO full radiative transfer calculations at Bornholm Basin~~

MOMO simulations were performed at relatively high angular resolution (twenty-seven angles in the atmosphere between 0 and 88 degrees plus nine additional angles in the ocean to cover the angular domain of total internal reflection) to allow for an accurate calculation of the in-water light field. Up to 120 terms were used for the Fourier expansion of the azimuth dependence of the light field. The oceanic vertical structure in MOMO has been chosen identical to the ROMS-Bio-Optic vertical structure, i.e., the light field has been calculated at the thirty ROMS-Bio-Optic layer boundaries located between 0 and ca. 90 m. Absorption and scattering coefficients for phytoplankton, CDOM, and detritus are taken directly from ROMS-Bio-Optic output. Spectral resolution was done in steps of 5 nm between 400 nm and 700 nm. Two Fournier-Forand phase functions (Fournier and Forand, 1994; Freda and Piskozub, 2007) with differing backscattering to scattering ratios have been applied to phytoplankton (bb/b = 0.001) and detrital material (bb/b = 0.1), in line with phase functions measured by Siegel et al. (2005) for various Baltic Sea coastal waters. Seasonal heating rates were derived from MOMO simulations at the Bornholm Basin location and compared to the corresponding fluxes from ROMS-Bio-Optic in order to assess the suitability of the simplified treatment of radiative transfer in the latter and the implications of not resolving the full directionality of the light field therein. MOMO results are presented for the 38° solar incident zenith angle, representative of late spring to mid-summer in the Western Baltic Sea (Figure 12).

~~MOMO simulations were performed over a range of solar zenith angles representative of seasons in the Western Baltic Sea using phytoplankton, CDOM and detrital absorption and scattering coefficients modelled using ROMS Bio Optic. Phase functions measured by Siegel et al. (2005) for various Baltic Sea coastal waters indicate that the Baltic Sea in general has a relatively low backscatter. Seasonal heating rates were derived from ROMS Bio Optic at the Bornholm Basin location and from comparable MOMO simulations in order to assess the suitability of the simplified treatment of radiative transfer in ROMS Bio Optic and the implications of not resolving the full directionality of the light field therein.~~

2.5 4 In situ and remotely sensed dataModel evaluation strategy and supporting data

Evaluation of our model output was carried out primarily at the Oder Bank, Darß Sill, Arkona Sea and Bornholm Basin sites within our model domain. These have been previously discussed in section 2.1 and are shown as blue dots in figure 3.

Three aspects of our model results were examined, as follows:

1. Seasonal cycle of modelled temperature versus observations at four locations. Darß Sill and Arkona Sea mooring data shown in Figure xx, middle panel, were obtained from the BSH (Bundesamt für Seeschifffahrt und Hydrographie) MARNET mooring database. SST data shown in Figure 3, right panel, were obtained from NOAA OI SST V2 High Resolution Dataset (Huang et al., 2021).

2. Model surface chlorophyll-a, phytoplankton and non-algal particulate absorption at 443 nm, and the diffuse attenuation coefficient at 490 nm, are compared with the Sentinel 3 Ocean and Land Colour Instrument, OLCI Level 3 300m data products (https://doi.org/10.48670/moi-00294) on two consecutive clear days in May 2018 when a bloom event occurred. Modelled monthly mean CDOM absorption is compared with MERIS-derived and in situ measurement-derived seasonal climatologies (Rohrenbach, 2019; see Appendix B for details). Seasonal phytoplankton and non-algal particle absorption (CDOM + detritus) at 440/442 nm are compared with seasonal estimates from Meler et al. (2016).

3. Heating rate estimates at Bornholm Basin derived from ROMS-Ecosim/BioOptic diagnostic calculations are compared with heating rate estimates derived from comparable full radiative transfer calculations using MOMO.

In situ observations and remotely sensed data from the MERIS ocean colour archive of CDOM absorption at 443 nm were used to develop a climatology of CDOM absorption with which to evaluate our modelled estimates of seasonal CDOM absorption. Below, the source and processing of the different data sets are briefly described.

2.5.1 In situ data

A time series (1994 - 2017) of in situ observations of CDOM absorption at 443 nm was reprocessed into seasonal means for our study area (Figure 1). This data set was collected as a result of the implementation of numerous research projects and statutory research programs conducted by the Remote Sensing Laboratory at the Institute of Oceanology, Polish Academy of Sciences (IOPAN), Sopot Poland in the whole Baltic Sea. The main aim of the study on CDOM optical properties was the assessment of its temporal and spatial variability (Kowalczuk and Kaczmarek, 1996, Kowalczuk, 1999) and its relation to hydrodynamic conditions and Baltic Sea productivity (Kowalczuk et al., 2006). As the primary goal of this research was the development and validation of ocean colour remote sensing algorithms (Kowalczuk et al., 2005a), the vast majority of samples for determination of CDOM absorption spectrum were collected in the surface layer. However, since 2014, samples were also collected within the water column, depending on the thermohaline stratification of water masses and depth distribution of autotrophic protists, in order to better resolve the impact of non-

linear processes (i.e. photo-degradation, autochthonous production by phytoplankton, diffusion from bottom sediments) influencing CDOM optical properties (Kowalczuk et al., 2015). The sampling program is conducted in the whole Baltic Sea and is designed to resolve the spatial variability of the CDOM absorption coefficient. We use a subset of this time series located in our study area (Figure 1). Most of the samples were taken in spring and autumn, with a smaller number of samples collected in winter and summer mostly due to adverse weather conditions or unavailability of research vessels in summer months. Water samples were collected by Niskin bottle and were filtered first through acid washed Whatman glass fibre filters (GF/F, nominal pore size 0.7 mm). The water was then passed through acid washed membrane filters with 0.2 mm pore to remove fine sized particles. From 2014 until the present, water for CDOM absorption spectra were gravity filtered directly from Niskin bottles through Millipore Opticap XL4 Durapore filter cartridge with nominal pore size 0.2 μm. Filtered water was kept in acid washed amber glass 200 ml sample bottles until spectrophotometric analysis, which was performed with use of various models of bench top research grade, double beam spectrophotometers both in land base laboratory (Kowalczuk and Kaczmarek, 1996; Kowalczuk, 1999) and on the ship (Kowalczuk et al., 2005a,b, 2006). The cuvette pathlength was 5 or 10 cm depending on the spectrophotometer model. MilliQ water was used as the reference for all measurements. The absorption coefficient aCDOM(λ) was calculated using Eq. (11) as follows:

$$a_{CDOM}(\lambda) = \frac{2.303A(\lambda)}{L} \tag{11}$$

where L is the optical path length, A is the absorptance (the flux that has been absorbed) and the factor 2.303 is the natural logarithm of 10.

The whole CDOM absorption data base in the IOPAN repository, collected between 1994 and 2017, was reprocessed to calculate the spectrum slope coefficient, S. A nonlinear least squares fitting method using a Trust Region algorithm implemented in Matlab was applied (Stedmon et al., 2000, Kowalczuk et al., 2006) in the spectral range 300-600 nm, using Eq. (12) as follows:

$$a_{CDOM}(\lambda) = a_{CDOM}(\lambda_0)e^{-S(\lambda_0 - \lambda)} + K \tag{12}$$

where λ_0 is 350 nm, and K is a background constant that allows for any baseline shift caused by residual scattering by fine size particle fractions, micro air bubbles or colloidal material present in the sample, refractive index differences between sample and the reference, or attenuation not due to CDOM. The parameters aCDOM (350), S, and K were estimated simultaneously via non-linear regression using Eq. (12).

24

3 Results

In section 3.1, we show the results from the biofeed experiment which includes the feedback from OSC-induced heating into the hydrodynamic solution. In section, 3.2 we show the difference between the biofeed experiment and the nobiofeed experiment where no feedback from OSC-induced heating is included in the hydrodynamic solution.

3.1 Seasonal cycle of temperature and the inherent and apparent optical properties of OSCs at Oder Bank, Darß Sill, Arkona Sea and Bornholm Basin in Western Baltic Sea

The modelled versus observed annual cycle of temperature at the different locations are shown in Figure 34. High resolution temporal and vertically resolved observations for 2018 were only available at Darß Sill and Arkona Sea sites (middle plots, Figure 34). , the white triangles in the Arkona Sea observation plot indicate periods where observations are missing from the time series). Oder Bank and Darß Sill are shallow, well-mixed locations, where seasonal warming and cooling of the whole water column takes place between May and October. At the deeper Arkona Sea and Bornholm Basin locations, the onset of seasonal stratification sets in early May and starts to break down in late OctoberSeptember. Intense summertime warming late July, early August (SST ~ 25°C) leads to a deepening of the thermocline from c. 20 m to the seafloor at Arkona Sea and to c. 38 m at Bornholm Basin. At Arkona Sea, the model captures observed summertime baroclinic inflows between 15 and 30m depth. These inflows are intrusions of deep, saltier, cool water which are pushed over the Drogen and Darß Sills into the deeper Arkona Sea. Due to the estuarine nature of Baltic Sea circulation, these inflows not unusual in the Western Baltic Sea (Fennel and Sturm, 1992). Overall, there is very good agreement between the modelled biofeed results and observed temperature fields at all locations, especially the sea surface temperature (see Table 2 1 for r^2, RMSE and BIAS statistics).
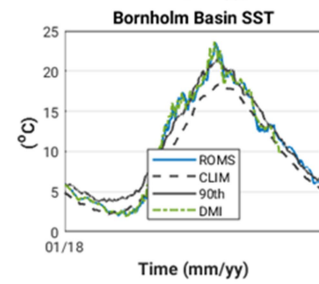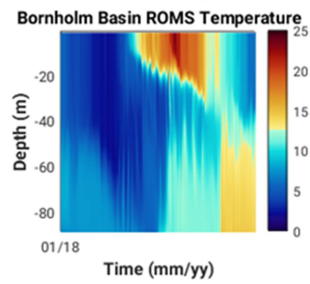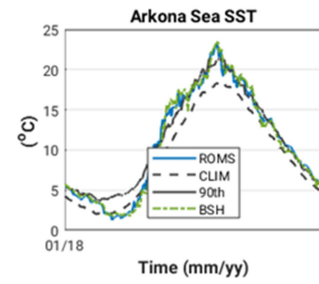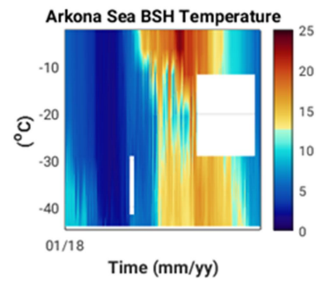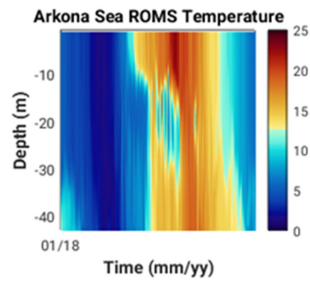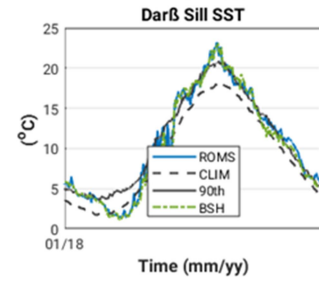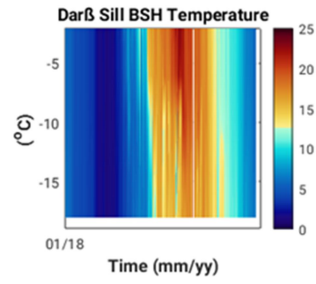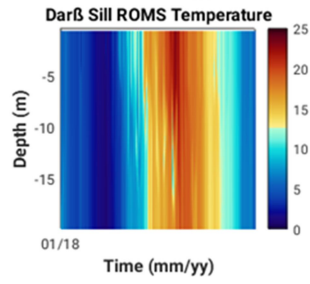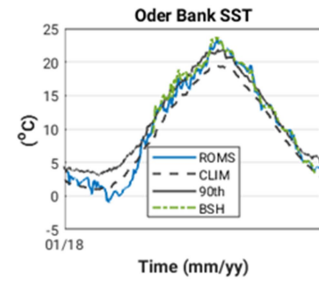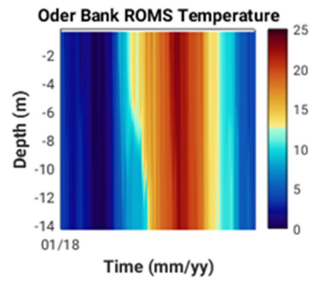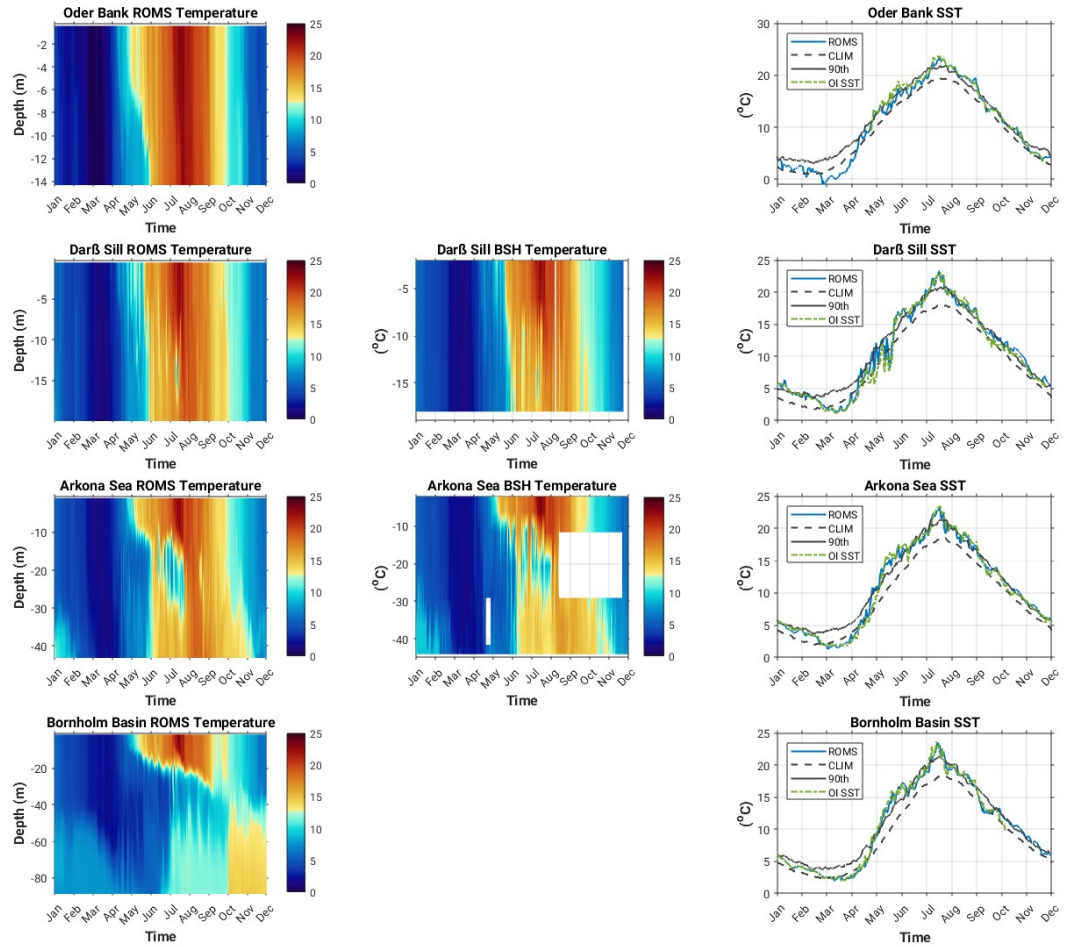
Figure 34: Modelled (left) versus observed (middle) annual cycle of temperature and sea surface temperature (right) in 2018 at Oder Bank, Darß Sill, Arkona Sea and Bornholm Basin. (see text for detailsLegend abbreviations: ROMS = model output; CLIM = 30 year climatological mean calculated from OI SST data set; 90th = 90th percentile of the 30 year climatological mean (CLIM); OI SST = 2018 daily optimum interpolation sea surface temperature (Huang et al., 2021)).

This is especially important as 2018 was a year where two significant marine heat waves (defined as periods where the surface temperature exceeds the 90th percentile of the 30 year local mean for longer than 5 days) took place in May - June (38 days) and July – August (32 days). This result confirms the importance of accounting for the contribution of OSCs to the transfer of light energy.

Table 21: Model versus ~~observations~~ observed sea surface temperature (°C) statistics.

	r^2	RMSE	BIAS
Oder Bank	0.98	0.025	0.0017
Darß Sill	0.98	0.020	-0.0010
Arkona Sea	0.99	0.016	-0.0010
Bornholm Basin	0.99	0.005	0.0003

3.2 Inherent and apparent optical properties of OSCs at Oder Bank, Darß Sill, Arkona Sea and Bornholm Basin in Western Baltic Sea

OLCI, level 3 products of chlorophyll a, phytoplankton and non-algal particle absorption at 443 nm, and the diffuse attenuation coefficient at 490 nm, at 300 m resolution are shown in Figure 5 for two consecutive days in May 2018. Comparable modelled output is shown in Figure 6. The white cross marks on the plots represent the position of the different analysis locations where matchups between the OLCI data and our model output have been extracted. These are reported in Table 2.
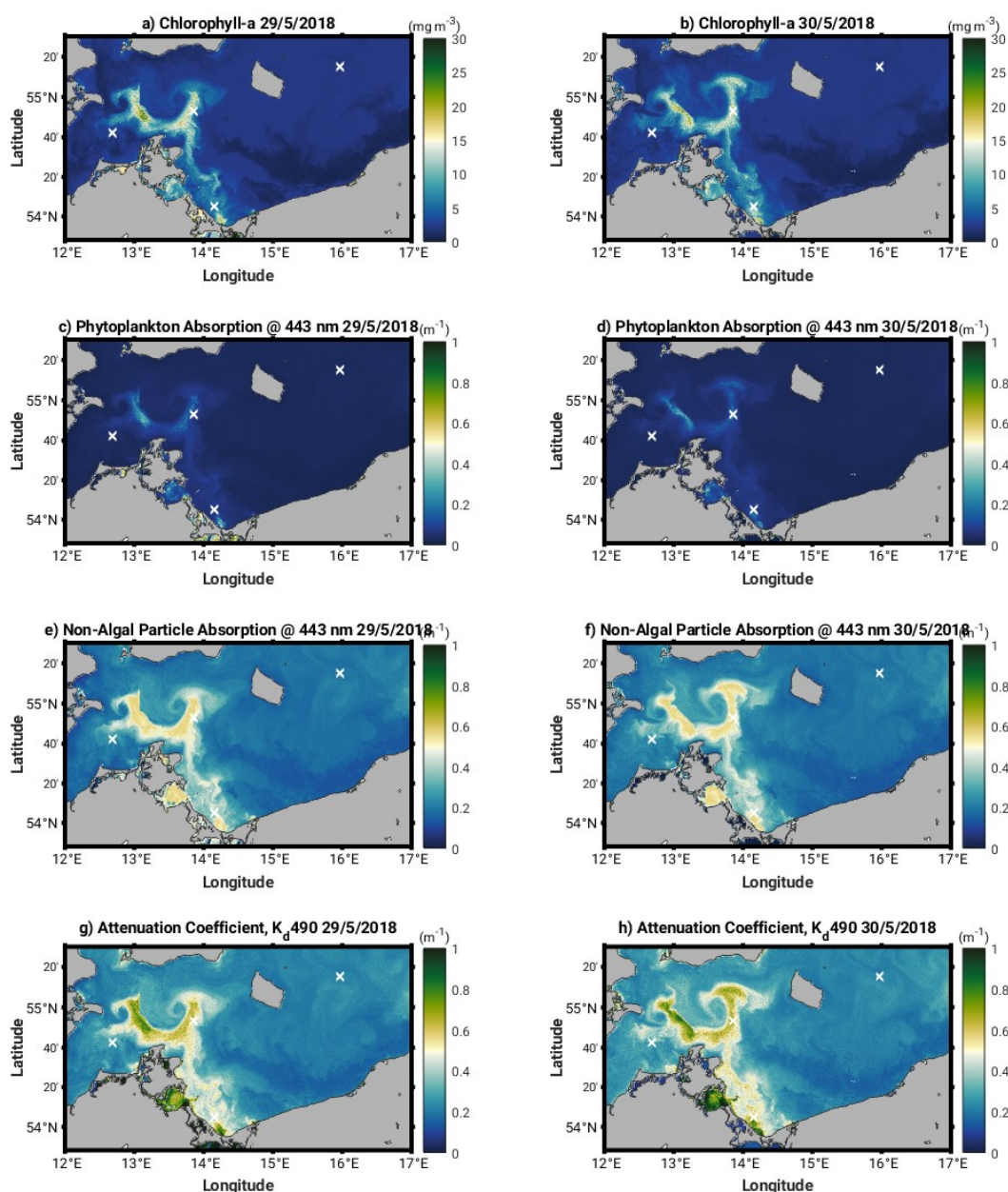
Figure 5: OLCI Level 3 300 m resolution chlorophyll-a (a-b), phytoplankton absorption at 443 nm (c-d), non-algal particle absorption at 443 nm (e-f) and diffuse attenuation coefficient at 490 nm, K_d490 (g-h) on 29th and 30th May 2018.
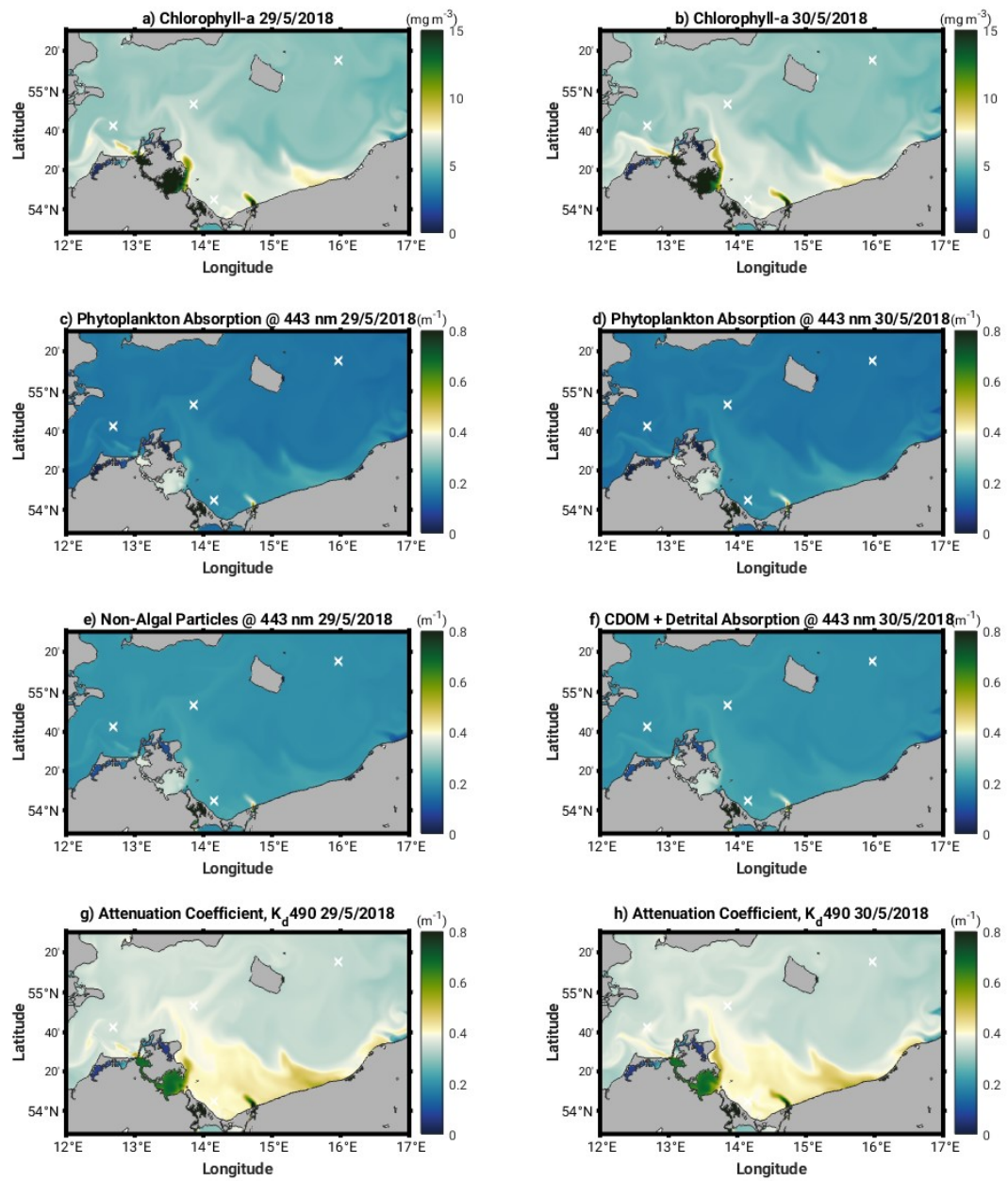
Figure 6: Modelled chlorophyll-a (a-b), phytoplankton absorption at 443 nm (c-d), non-algal particle absorption at 443 nm (e-f) and diffuse attenuation coefficient at 490 nm, K_d490 (g-h) on 29th and 30th May 2018.

Table 2: OLCI versus model matchup values for Chl-a, phytoplankton (aPhy) and non-algal particle (aNAP) absorption at 443 nm, and the diffuse attenuation coefficient at 490 nm, $K_d 490$.

	OLCI		Model		OLCI - Model	
	29/05/2018	30/05/2018	29/05/2018	30/05/2018	29/05/2018	30/05/2018
Darß Sill						
Chl-a (mg m^{-3})	2.17	2.38	3.21	3.63	-1.04	-1.25
aPhy (m^{-1})	0.04	0.04	0.16	0.17	-0.12	-0.13
aNAP (m^{-1})	0.24	0.22	0.21	0.21	0.03	0.01
$K_d 490$ (m^{-1})	0.28	0.25	0.36	0.40	-0.08	-0.15
Arkona Sea						
Chl-a (mg m^{-3})	6.49	10.26	3.39	3.31	3.10	6.95
aPhy (m^{-1})	0.08	0.09	0.17	0.17	-0.09	-0.08
aNAP (m^{-1})	0.42	0.51	0.21	0.21	0.21	0.30
$K_d 490$ (m^{-1})	0.44	0.53	0.38	0.37	0.06	0.16
Oder Bank						
Chl-a (mg m^{-3})	9.69	9.79	3.80	3.74	5.89	6.05
aPhy (m^{-1})	0.08	0.09	0.19	0.19	-0.11	-0.10
aNAP (m^{-1})	0.46	0.52	0.23	0.23	0.23	0.29
$K_d 490$ (m^{-1})	0.50	0.61	0.41	0.40	0.09	0.21
Bornholm Basin						
Chl-a (mg m^{-3})	2.25	2.24	3.00	3.03	-0.75	-0.79
aPhy (m^{-1})	0.03	0.04	0.15	0.16	-0.12	-0.12
aNAP (m^{-1})	0.18	0.21	0.20	0.20	-0.02	0.01
$K_d 490$ (m^{-1})	0.21	0.23	0.34	0.34	-0.13	-0.11

The matchups (Table 2) highlight how we can only reasonably compare OLCI and model output at the Darß Sill and Bornholm Basin locations, as the bloom event evident in the OLCI data in Arkona Sea and Oder Bank (Figure 5) is not captured in the model. At these locations, Chl-a and NAP absorption are all underestimated by the model, by as much as 7 mg m^{-3} and 0.3 m^{-1}, respectively. Phytoplankton absorption is slightly overestimated in the model at all locations, but the values are in better agreement with the OLCI data (within 0.1 m^{-1} difference range), as are the modelled non-algal particle absorption values at Darß Sill and Bornholm Basin (within 0.03 m^{-1} difference range). Modelled $K_d 490$ also compares reasonably well with the OLCI data at all locations (within 0.2 m^{-1} difference range). We do not expect the model to capture the dynamic bloom event observed by OLCI without further tuning or data assimilation. As it stands, there is good agreement between the model and OLCI data with the background values at Darß Sill and especially, at Bornholm Basin which give us confidence in the model performance and supports the selection of Bornholm Basin for further evaluation of the heating rates and air sea fluxes.

We also compared modelled monthly mean CDOM absorption with MERIS-derived and in situ-derived climatologies, as well as seasonal phytoplankton and non-algal particle absorption with seasonal estimates from Meler

et al. (2016). Modelled monthly mean surface CDOM absorption is underestimated as compared to the MERIS-derived climatological CDOM absorption (Figure 7b) but is in better agreement with the seasonal observed estimates of Meler et al. (2016) (Figure 7c). There is also good agreement between modelled seasonal phytoplankton absorption and the seasonal estimates of Meler et al. (2016), especially in spring and summer (Figure 7d).
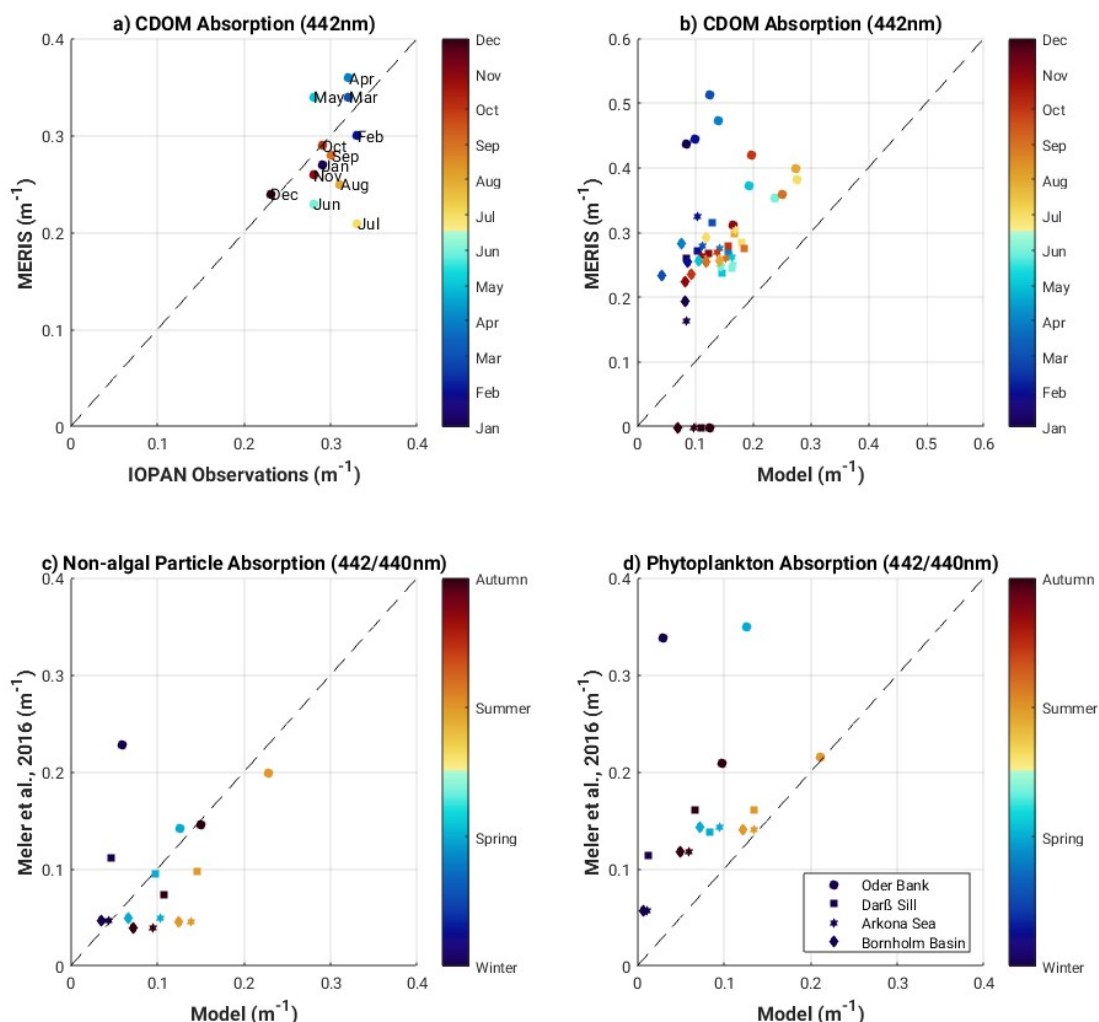

Figure 7Figure A1: (a) MERIS and in situ monthly climatology of surface CDOM absorption (mean value calculated over Western Baltic Sea region shown in Figure 21); (b) mean monthly surface CDOM absorption at model stations and matching MERIS locations; seasonal mean surface non-algal particle absorption (CDOM+detritus) (c) and phytoplankton absorption (d) at model stations compared with similar water type values found in Meler et al. (2016).

Modelled seasonal spectral surface absorption from the 3D Western Baltic Sea experiment for phytoplankton, CDOM and detritus is shown for Oder Bank, Darß Sill, Arkona Sea and the Bornholm Basin (Figure 48) show typical absorption characteristics for the individual constituents. CDOM and detritus have high absorption values at the blue end of the spectrum, while phytoplankton shows two maxima, one between 440 nm and 490 nm and a smaller one around 670 nm. There is a clear seasonal pattern for each of the constituents, with spring and summer being peak

784 seasons for phytoplankton blooms, and summer and autumn favouring increased CDOM and detrital absorption.
785 Considerable variability in absorption characteristics is evident between the locations. The highest absorption for all the
786 constituents is seen at the coastal Oder Bank location, which is strongly influenced by riverine inputs from the Oder
787 River. There is a decreasing gradient, especially in CDOM and detrital absorption, moving from the coastal zone to the
788 offshore regions. The summer phytoplankton bloom in the Arkona Sea has a higher peak than the Darß Sill.

789 CDOM, detritus and phytoplankton specific absorption curves intersect around 442 nm, making this an
790 interesting wavelength to explore further with respect to the impact of these constituents on the vertical distribution of
791 absorption and the downward attenuation and irradiance fields.

792 The vertical profiles of phytoplankton, CDOM and detrital absorption at 442 nm (Figure 5 9) show the vertical
793 extent of water constituent absorption to be the full water column at Oder Bank and Darß Sill and between 15 and 20 m
794 depth at Arkona Sea and Bornholm Basin. In spring and especially in summer, phytoplankton dominate sub-surface
795 absorption at all locations, followed by CDOM and then detrital absorption.

796 The spectrally-resolved surface downward attenuation (K_d) and downward irradiance (E_d) at each of the
797 locations shown in Figure 6 10 reflect the seasonal impact of the water constituent absorption and solar irradiance.
798 Irradiance at the surface peaks in summer and is at its lowest in winter, as expected. The slight modification of
799 downwelling irradiance intensity in the Baltic Sea depends on atmospheric conditions. Results of direct measurements
800 and local parameterizations of radiative transfer models summarised by Dera and Woźniak (2010) (and initially reported
801 by Rozwadowska and Isemer (1998) and Isemer and Rozwadowska (1999)), indicate that observed monthly averaged
802 solar irradiance intensities at the sea level in the Baltic Sea are always lower than model estimates based on the clear
803 sky assumption. Atmospheric conditions have a regional and seasonal impact on observed solar irradiance entities e.g.
804 in the southern Baltic Proper and western Baltic Sea, the long-term monthly average for E_d at the surface in May is only
805 4.8 and 1.8 Wm^{-2}, respectively, lower from E_d intensity observed in June in both regions. This is caused by much lower
806 cloud cover over Baltic Sea observed in May than in June. Our monthly mean modelled surface irradiances converge
807 with those reported in Dera and Wozniak (2010) (Appendix D, Figure D1). We applied a constant fraction of 0.3 cloud
808 cover while in Dera and Wozniak (2010), the clear sky assumption was applied. This would explain why our irradiances
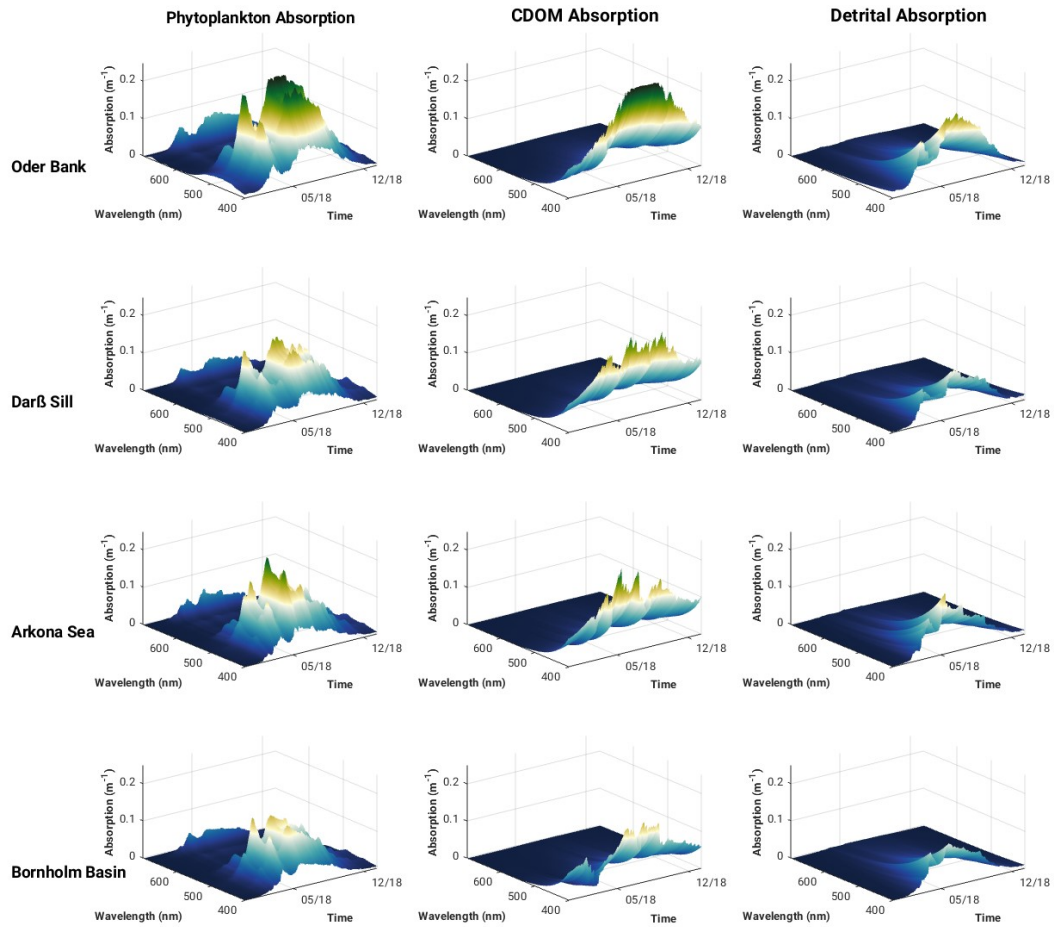809 are lower than Dera and Wozniak (2010), especially in May, June and July.

Figure 48: Surface spectral phytoplankton, CDOM and detrital absorption at Oder Bank, Darß Sill, Arkona Sea and Bornholm Basin in 2018 from ROMS-Bio-Optic 3D Western Baltic Sea model experiment.
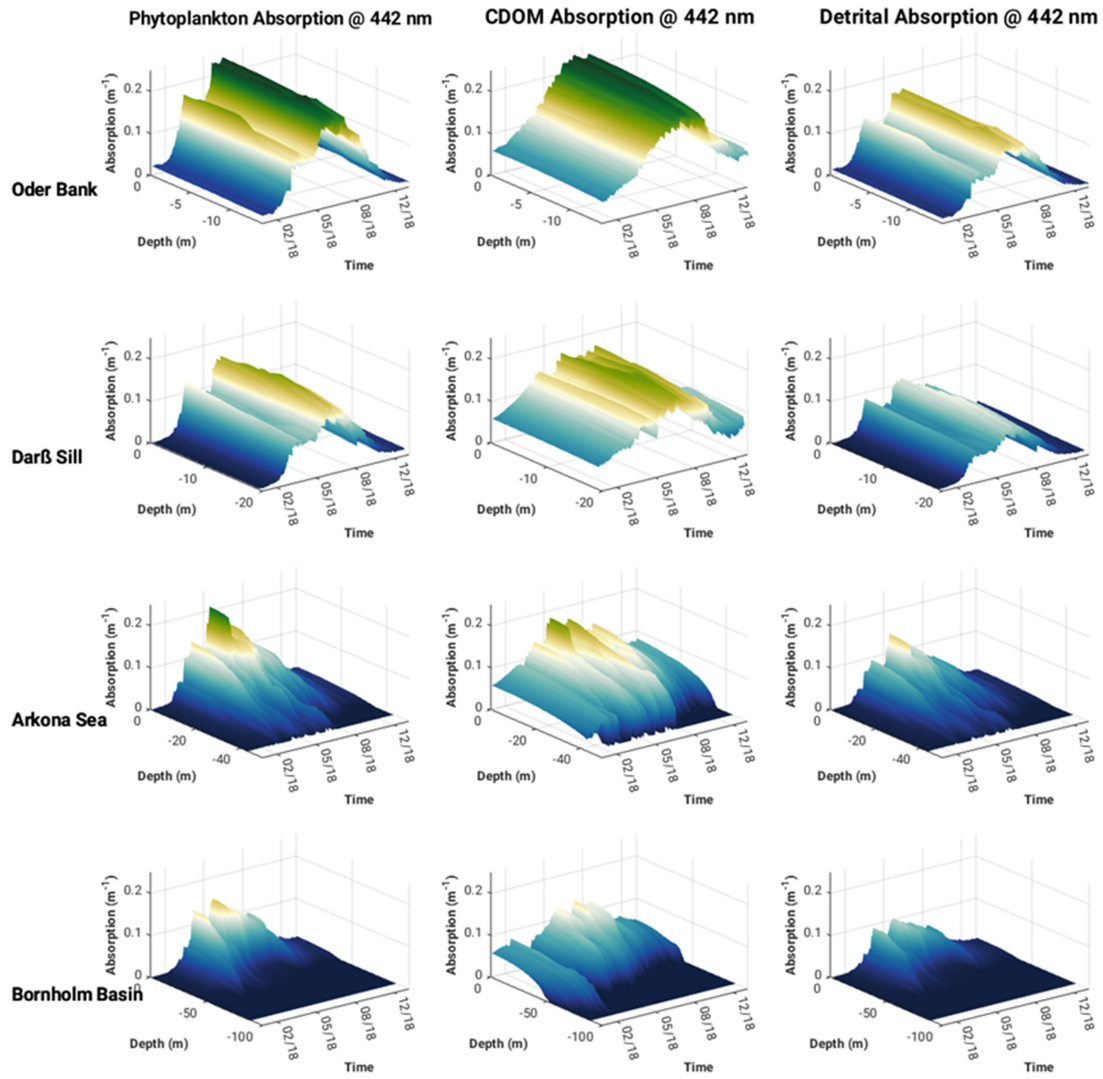
Figure 95: Vertical structure of phytoplankton, CDOM and detrital absorption at 442 nm at Darß Sill, Arkona Sea, Oder Bank and Bornholm Basin in 2018 from ROMS-Bio-Optic 3D Western Baltic Sea model experiment.
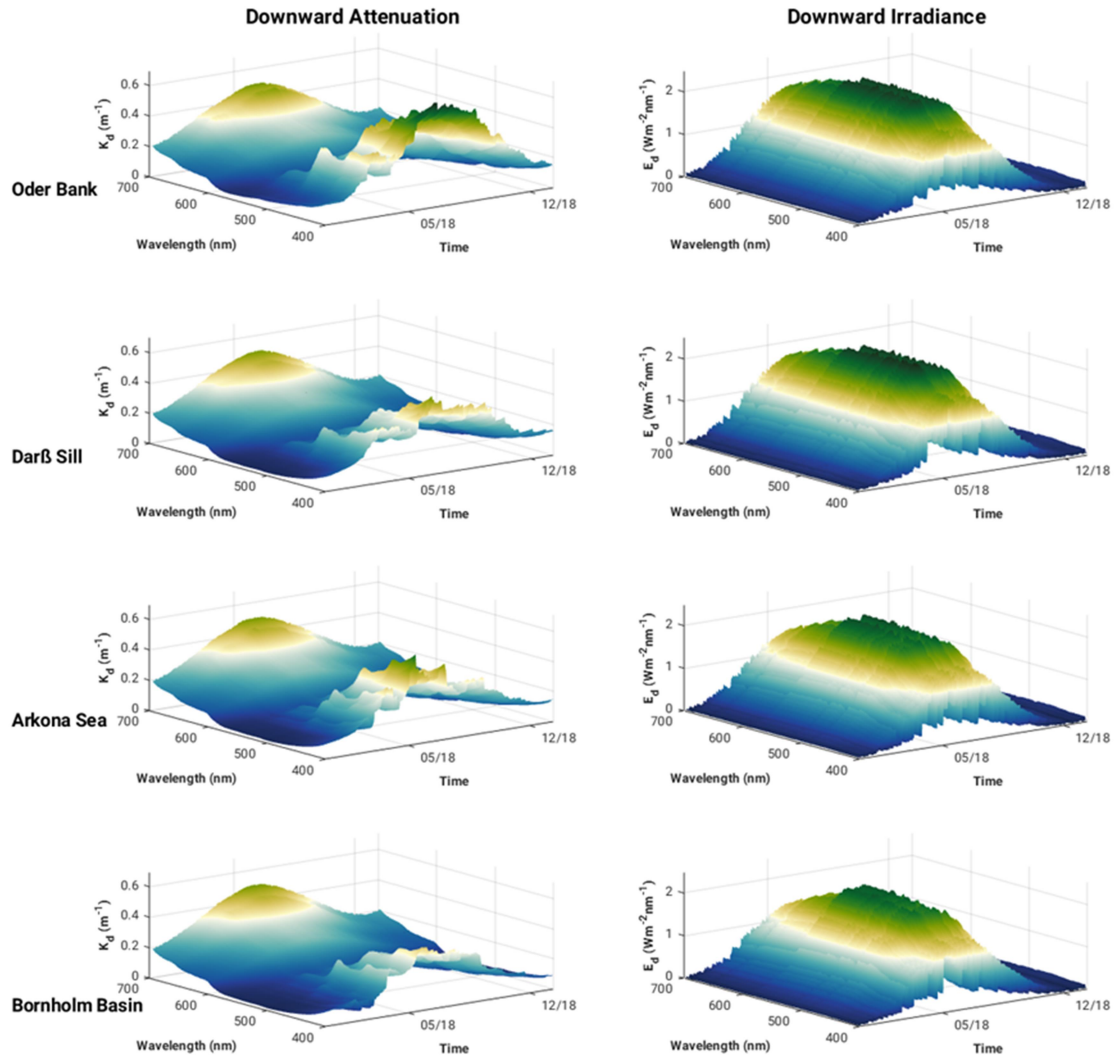
Figure 610: Surface spectral downward diffuse light attenuation and downward irradiance at Oder Bank, Darß Sill, Arkona Sea and Bornholm Basin in 2018 from ROMS-Bio-Optic 3D Western Baltic Sea model experiment.

Variability in the surface layer attenuation is greatest between 400 and 550 nm, especially during the stratified spring, summer and autumn seasons reflecting the seasonal dynamics of phytoplankton, CDOM and detritus. Vertical profiles of K_d and E_d at 442 nm (Figure 711) show light penetrating deeper in winter, indicating relatively well-mixed (clear) waters, contrasted by seasonally stratified waters in spring, summer and autumn. Variability between the locations is also much higher during these seasons revealing the different influence of constituents at these locations, for example, the impact of the spring and summer phytoplankton blooms at Oder Bank and Arkona Sea on attenuation. (High attenuation values at the red end of the spectrum are mostly related to the absorption of pure water itself).
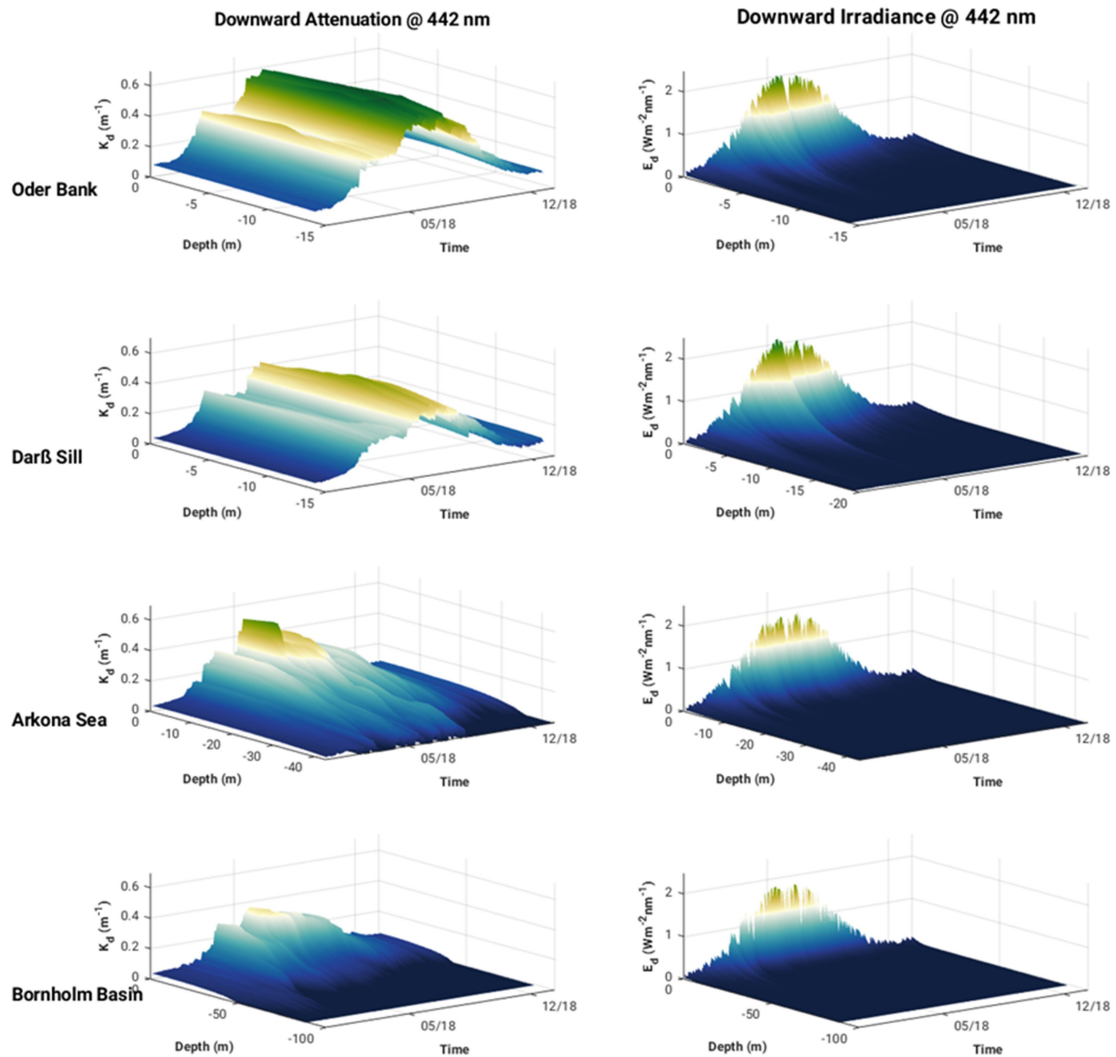
Figure ~~7~~11: Vertical structure of downward diffuse light attenuation and downward irradiance at 442 nm at Oder Bank, Darß Sill, Arkona Sea and Bornholm Basin in 2018 from ROMS-Bio-Optic 3D Western Baltic Sea model experiment.

It should be noted that seasonal and spatial variability in the concentration of optically significant water constituents impacts not only the penetration of solar energy into the water column, but also influences the spectral properties of the underwater light field. Elevated absorption by CDOM and phytoplankton pigments in the spring and summer at the Oder Bank, Darß Sill and Arkona Sea causes a red shift in the solar irradiance maximum transmission waveband to 570 nm from 500 nm estimated for the Bornholm Basin (Figure ~~6~~10). This is consistent with observations reported by Kowalczuk et al. (2005a) who reported a shift in solar irradiance maximum transmission waveband from 550 nm in the Baltic Proper to 575 nm in Pomeranian Bay and Gulf in Gdansk. An even bigger shift in the solar

irradiance maximum transmission waveband was observed between Atlantic Ocean coastal water off the west coast of Ireland (maximum solar irradiance transmission at 490 nm) and Baltic Sea in Gulf of Gdansk (maximum solar irradiance transmission at 570 nm). This shift was attributed to elevated CDOM absorption, which was c. two times higher in the Baltic Sea compared to coastal Atlantic Ocean, while the chlorophyll-a concentration was at a similar level in both regions (Darecki et al., 2003).

3.3 Heating rates and surface heat fluxes

The vertical and temporal evolution of water constituent-induced heating rates at each of the locations is shown in Figure 812. Maximum heating rates occur late spring and mid-summer and are between 0.8 and 0.9 K $m^{-1}d^{-1}$ at Oder Bank and between 0.4 and 0.8 K $m^{-1}d^{-1}$ at the other locations. Vertical profiles of two heating rate maxima in May and July indicate approximately 70% of the water constituent-induced heating is contained within the top 5 m, and decreases exponentially to zero by 10 to 15 m depth.

We compared the Bio-Optic heating rate estimates at Bornholm Basin with a comparable full radiative transfer calculation by MOMO for the two heating rate maxima events in May and June (Figure 812, bottom right). Bornholm Basin is chosen as the evaluation site for the heating rate calculations because the seasonal cycle of the heat balance there can be approximated as a 1-dimensional balance between the penetration of solar radiation and vertical mixing (Gnanadesikan et al., 2019) and advective and diffusive terms will be relatively small. The main difference between the two calculations, Bio-Optic and MOMO, is that the MOMO takes into account the full directionality of the light field while Bio-Optic does not. There are differences in the seasonal heating rate results between the two approaches but they are not so large. At the surface, the Bio-Optic estimates are 0.3 K $m^{-1}d^{-1}$ smaller in spring and 0.25 K $m^{-1}d^{-1}$ smaller in summer than the MOMO estimates. In the MOMO calculations, most of the water constituent-induced heating (c. 80 %) is contained within the top 2 m, and this decreases exponentially more rapidly than Bio-Optic to zero by 5 m depth.

We find that by accounting for the full directionality of the light field, as shown by the case investigated by MOMO, the impact water constituents have on the heating rates is contained within the top 2 to 3 m, consistent with the findings of Soppa et al. (2019). However, MOMO may be overestimating the actual magnitude of water constituent-induced surface heating rates as none of the other physics (i.e. advection, diffusion) and environmental forcing represented in the Bio-Optic experiments, are taken into account in MOMO. It could also be that the algorithm used to calculate K_d in Bio-Optic (Lee et al., 2005) is not optimal for the conditions in the Baltic Sea (we elaborate this point further in the discussion).
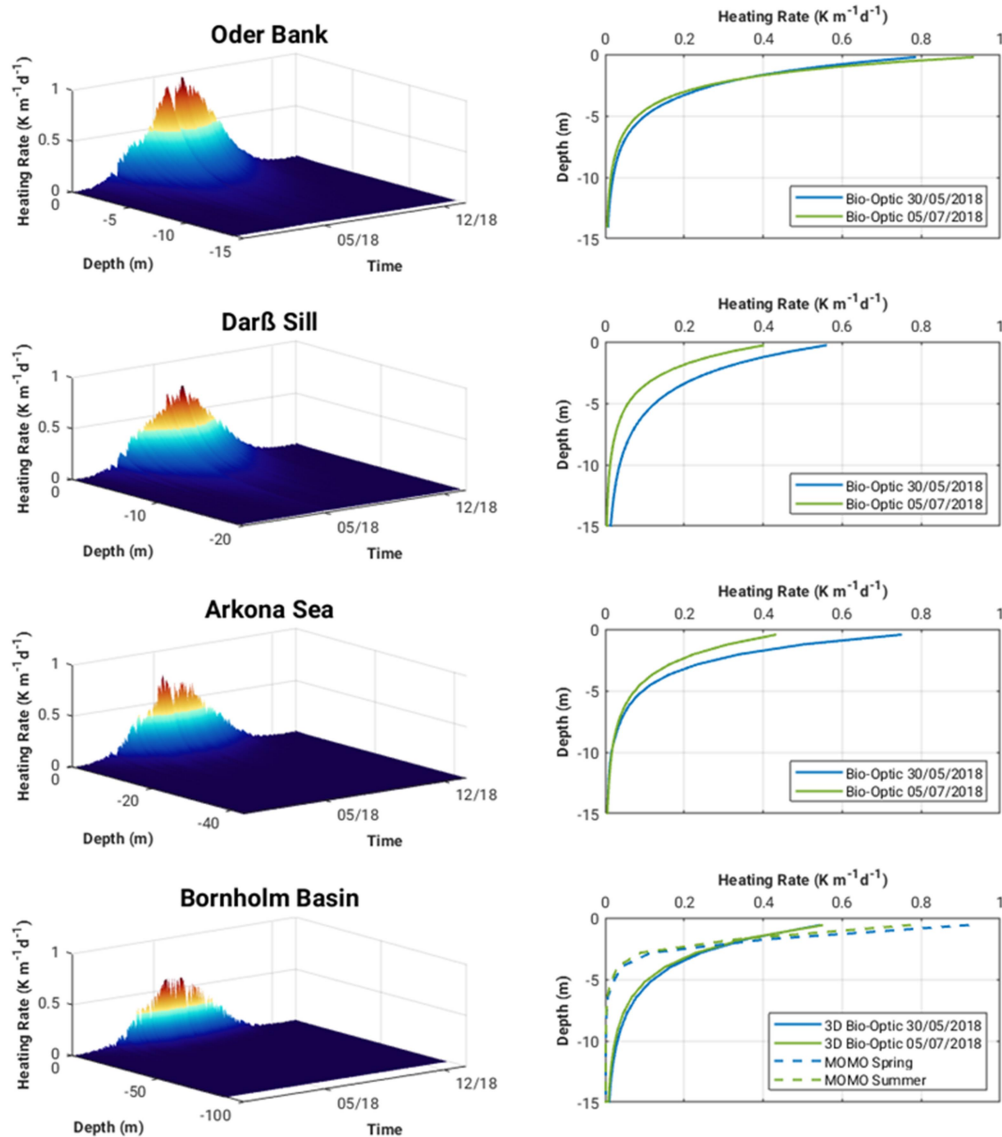
Figure 812: Surface heating rates (left panel) and vertical profiles of two heating rate maxima in May and July 2018 (right panel) for at Oder Bank, Darß Sill, Arkona Sea and Bornholm Basin.

Figure 9 13 shows the temperature and chlorophyll-a anomalies (biofeed minus nobiofeed experiments) for selected days during the productive period at Bornholm Basin. Accounting for the feedback of OSC-induced heating in the hydrodynamic solution has the effect of increasing the surface layer (c. top 10m) water temperature by between 0.1 and 0.2°C in spring and late summer, and as much as 0.6°C mid-summer. Below the thermocline, the water temperature is cooler by 0.1 to 0.2°C. Differences in the thermal structure when the feedback is accounted for impacts the development, transport and fate of phytoplankton biomass. This consequence is seen in differences in the chlorophyll-a

structure at different times during the productive period. ~~The increase in light~~ ~~In~~ in spring, ~~supports phytoplankton growth~~ ~~when the upper water column is stratifying, the~~ and increase ~~in~~s the surface temperature (due to both water and phytoplankton absorption) in the surface layer. ~~will stimulate production and increase the absorption of light by phytoplankton, thus~~Thus, ~~strongly reducing~~ the availability of light below the algae layer is strongly reduced and ~~.~~ ~~P~~phytoplankton ~~is~~ are restricted within the shallow mixed layer with more availability of light, which will in turn increase surface heating. The net effect is more biomass production in the surface layer at the beginning of the spring bloom in biofeed compared to nobiofeed. As nutrients become depleted in the surface layer and the supply of nutrients from deeper waters is inhibited by the stronger thermocline mid-summer, the net effect is less biomass production in the surface layer mid-summer in biofeed compared to nobiofeed. As the water column becomes less stable late August, and nutrients are mixed back into the surface, biomass production is larger again in biofeed compared to nobiofeed.
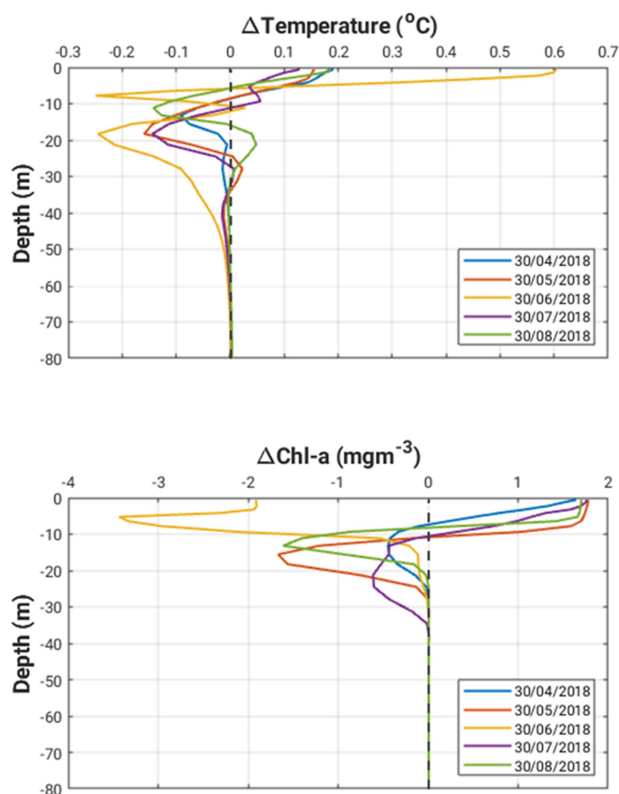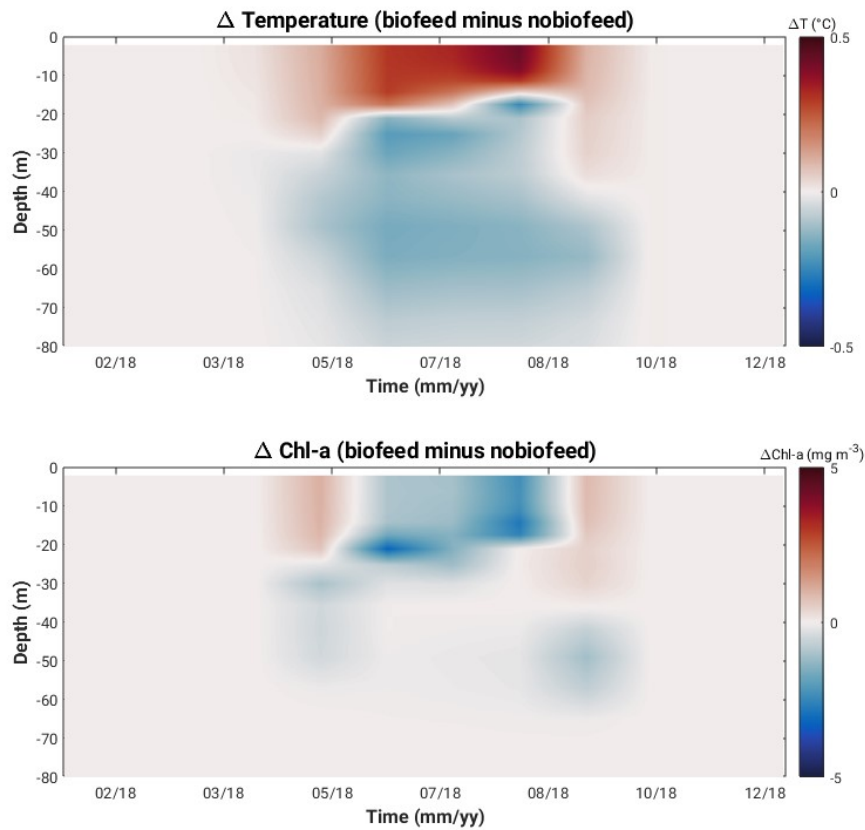
Figure 139: ~~Vertical profiles~~Hovmöller plots of temperature and chlorophyll-a anomalies (biofeed minus nobiofeed experiments) ~~during productive period~~in 2018 at Bornholm Basin.

The impact this has on surface heat fluxes during the productive period at Bornholm Basin is shown in Figure ~~10~~14. The increase in OSC-induced surface temperature captured in spring and summer lead to an increase in heat loss to the atmosphere, with the average difference for the period April to September being on the order of 5.2 Wm^{-2}. This is primarily a result of latent (2.6 Wm^{-2}) and sensible (1.7 Wm^{-2}) heat fluxes. Putting this into context with modelled estimates by Omstedt and Nohr (2004) of between 5 and 18 Wm^{-2} for the net annual heat losses in the Baltic Sea, indicates it may be important to consider OSC-induced heating rates in regional heat balance budgets.
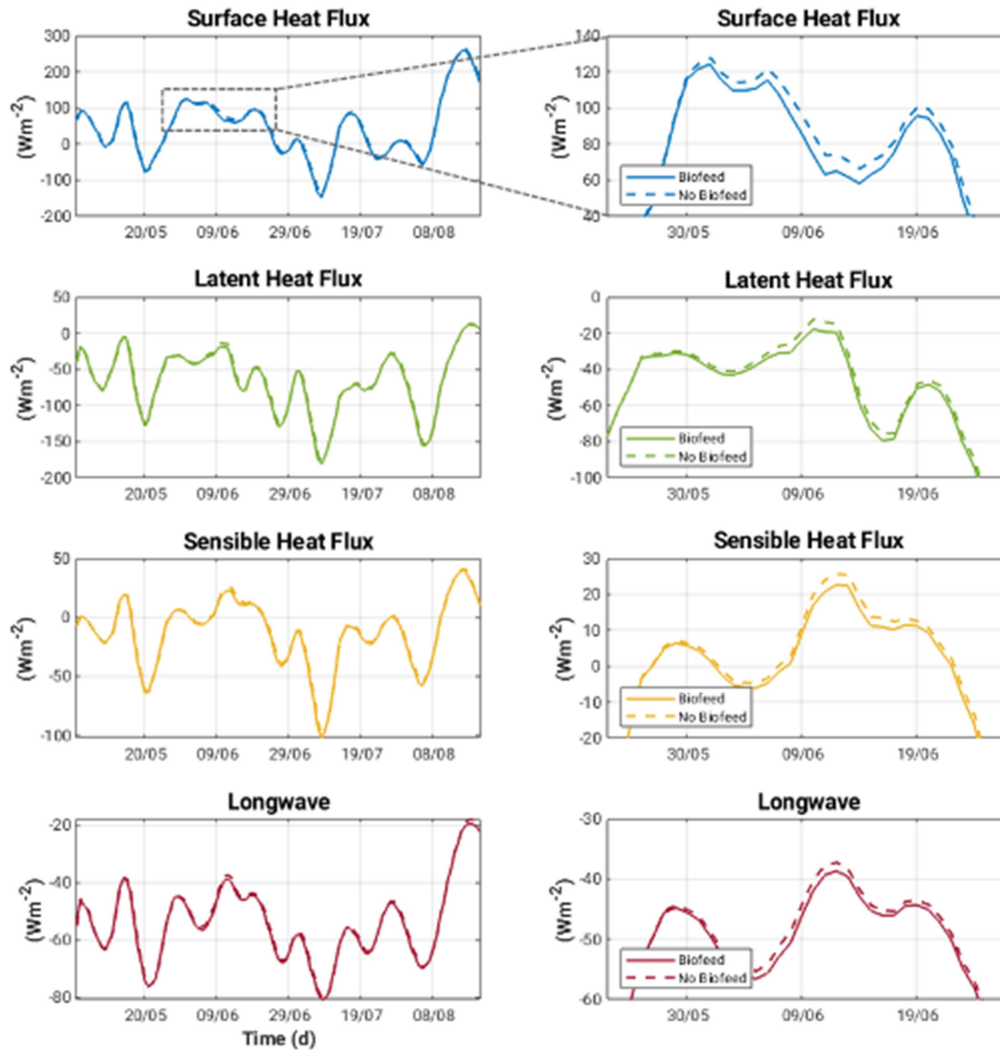
913
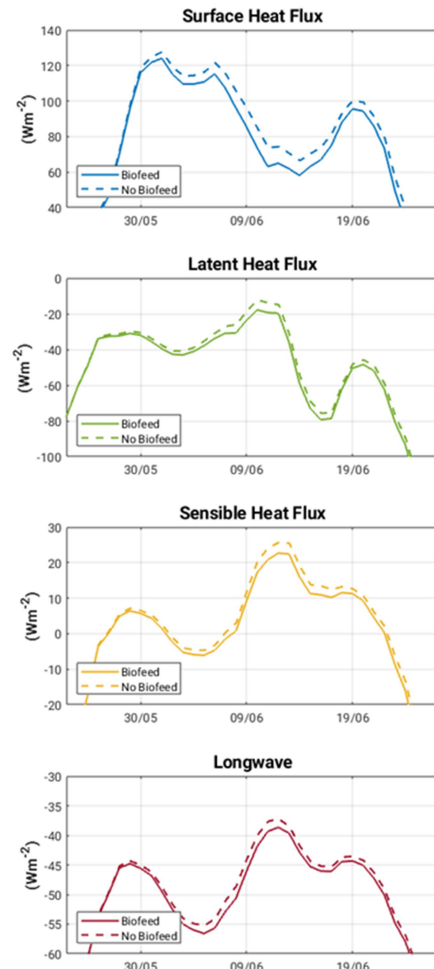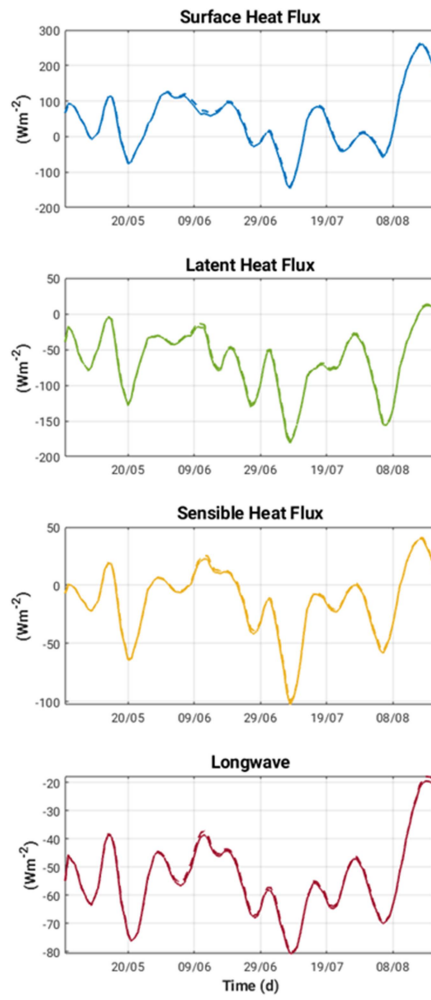
Figure 1014: Surface heat fluxes for both biofeed and nobiofeed experiments during the entire productive period, April to September, (left panel) and zooming in on the period where the difference in surface heat fluxes between experiments is greatest (area shown in rectangular box shown in top left panel)- at Bornholm Basin.

4 Discussion

Modelled seasonal and spatial changes in OSCs in the Western Baltic Sea have a small but noticeable impact on radiative heating in surface waters, especially in spring and summer as a consequence of increased absorption of light by phytoplankton and CDOM. Our modelled estimates for 2018 show phytoplankton dominating absorption in spring and summer, as a result of a succession of phytoplankton blooms, and CDOM dominating absorption in summer and autumn. Simis et al. (2017), found that phytoplankton pigment visibly influences $K_d(675)$ in spring and summer, while

absorption by CDOM at 412 nm can account for 38–70 % of the total OSC absorption in the area influenced by the Oder River in autumn. First order variability in CDOM absorption in the Baltic Sea is driven by terrestrial sources. Second order variability is driven by autochthonous DOM production during phytoplankton blooms and photodegradation. The spatial and temporal variability in our modelled OSC absorption at the different locations, especially in spring, summer and autumn, are in good agreement with seasonal observations for different water types in the Southern Baltic Sea reported by Meler et al. (2016a) (~~See appendix,~~ Figure A~~1~~7c,d). This is also bolstered by good agreement between the model and OLCI data match ups with the background values at Darß Sill and Bornholm Basin which give us confidence in the model performance. This is encouraging for future modelling studies of this nature, as more consistent, long term time series of the optical properties of the Baltic Sea are realised e.g. using automated measurement systems such as Bio-Argo floats equipped with a simple spectral radiometer. Such a strategy has been applied with significant success in the Mediterranean Sea (Terzić et al., 2019; Terzić et al., 2021a; Terzić et al., 2021b). We also find it encouraging that the (simplified) Bio-Optic and (full) MOMO radiative transfer heating rate estimates were somewhat comparable and informative. The directionality of the light field appears to be important to understand the depth of influence of water constituent-induced heating rates, while accounting for the spatial and temporal variability in the physics of the environment is important in determining the magnitude of the heating rates. However, we think further work is needed to optimise the Bio-Optic diffuse attenuation coefficient (K_d) algorithm for the Baltic Sea.

K_d which describes the transfer of light energy through the water column, also reflects the seasonal variability of water types, i.e. winter (well-mixed) versus spring, summer and autumn (seasonally stratified) and the influence of constituents in different water types during stratified seasons (i.e. spatial variability). Our results show a gradient in K_d and in heating rates which decreases as you move offshore. In late spring, at the Oder Bank, water constituent contribution to surface heating can be as much as 0.9 K m^{-1}d^{-1}, while at Darß Sill, Arkona Sea and Bornholm Basin, water constituent contribution to surface heating in spring and summer is less, between 0.4 and 0.8 K m^{-1}d^{-1}. Reports on the spectral properties, temporal and spatial variability of the diffuse attenuation coefficient in the Baltic Sea based on field observations are limited and date back to the early 2000s (Kratzer et al. 2003, Lund-Hansen, 2004, Darecki and Stramski 2004, Kowalczuk et al., 2005a, Lee et al., 2005). Darecki and Stramski (2004) have assessed that locally optimised satellite remote sensing algorithms for estimating $K_d(490)$ based on MODIS data yield the least uncertainty compared to other variables e.g. chlorophyll-a. However, information on the full K_d spectrum is needed to assess the individual impact of the most significant optical seawater constituents on surface heating rates. Until recently, the only solution was empirical or semi- analytical modelling based on either remote sensing data (Lee at al. 2005; Löptien and Meier, 2011; Alikas et al., 2015) or in situ measurements of apparent or inherent optical measurements (Gonçalves-Araujo and Markager, 2020). The most accurate estimation of K_d could be achieved by using the semi-analytical model, however, uncertainty in those estimates heavily depends on the local parametrization of the specific inherent optical properties which, in the Baltic Sea regions, have contrasting and highly variable seasonal cycles (Simis et al., 2017).

959 Kratzer and Moore (2018) concluded that the correct choice of the volume scattering phase function in the Baltic Sea

960 determines the accuracy of the prediction of inherent and apparent optical properties in the Baltic Sea region. CDOM

961 and suspended particles are the most significant optical constituents controlling water transparency. CDOM absorption

962 is regulated mostly by riverine discharge especially in coastal waters, however, under certain condition, CDOM

963 absorption in the Baltic Sea is statistically correlated with phytoplankton biomass (Kowalczuk et al., 2006, Meler at al.,

964 2016a). Particulate absorption and scattering is significantly correlated with phytoplankton biomass, which has a well-

965 defined seasonal and spatial pattern in the Baltic Sea (Meler et al., 2016b, Meler at al., 2017). By including a spectrally

966 resolved underwater light field in our model and diagnosing inherent and apparent optical properties, we are able to

967 resolve the full K_d spectrum and better understand the role different OSCs play in determining the temporal and spatial

968 variability in K_d and the impact on heating rates. Further optimisation of the Bio-Optic K_d algorithm for the Baltic Sea

969 is currently in progress.

970   Climate change scenarios for central Europe predict significant change in the precipitation regime, which will

971 be manifested in a shift in the seasonal distribution of precipitation: increased rainfall and decline in snowfall in winter,

972 persistent droughts in summer with episodic intensive thunderstorms (IPCC, 2022). Changes in the precipitation regime

973 coupled with an increase of mean temperatures will significantly impact the outflow of freshwater from the Baltic Sea

974 catchment into the marine basin itself (Meier et al., 2022). We could anticipate that the flux of terrestrial CDOM would

975 be affected most, because currently observed climatic changes in the southern part of Baltic Sea catchment have caused

976 mild winters with reduced numbers of frost days and almost a total reduction in snow fall. As a result, CDOM that was

977 previously immobilised in the frosted ground, streams and rivers, is now being transported to the sea in late winter and

978 spring. In the summer, a deepening minima of flows in rivers reduces CDOM input to Baltic Sea. Recent results by

979 Zabłocka (2017) indicate that the monthly averaged Vistula river flow maximum during the period 1993 to 1998

980 occurred in April, while from 2008 to 2010, this maximum shifted to March. As the Baltic Sea is warming at a rate up to

981 four times the global mean warming rate (Belkin, 2009), we can expect this trend in earlier river flow maxima to

982 continue and a higher contribution of CDOM to the absorption budget in winter and spring, as the chlorophyll-a

983 concentration (phototrophic protists biomass proxy) maximum still occurs in April (Stoń-Egiert and Ostrowska, 2022).

984   Changes in the hydrological regime and a reduction in mineral nutrient input (Łysiak-Pastuszak et al., 2004)

985 have noticeably impacted both phototrophic protists biomass and functional structure. Stoń-Egiert and Ostrowska (2022)

986 have reported a statistically significant decreasing trend of 2.11 % yr^{-1} of the total chlorophyll-a concentrations over last

987 two decades (1999 to 2018), with decreasing pigment markers for such protists groups as diatoms, dinoflagellates,

988 cryptophytes and green algae and an increase of cyanobacteria. As a consequence, primary production in the southern

989 Baltic Sea also declined in the period from 1993 to 2018, compared to its maximum in the late 1980s (Zdun et al., 2021).

990 Kahru et al. (2016) have also reported on changes in the seasonality in the Baltic Sea environment: the cumulative sum

991 of 30,000 $Wm^{-2}d^{-1}$ of surface incoming shortwave irradiance (SIS) was reached 23 days earlier in 2014 compared to 3

992 decades earlier; the period of the year when the sea surface temperature was at least 17°C has almost doubled (from 29

days in 1982 to 56 days in 2014); the period when $K_d(490)$ was over 0.4 m^{-1} increased from about 60 days in 1998 to 240 days in 2013 (quadrupled); the period when satellite-estimated chlorophyll of at least 3 mgm^{-3} has doubled from 110 days in 1998 to 220 days in 2013 and the timing of both the phytoplankton spring and summer blooms has advanced, with the annual chlorophyll maximum that in the 1980s corresponded to the spring diatom bloom in May has now shifted to the summer cyanobacteria bloom in July. It is interesting to note that we found two OSC-induced heating rate maxima in May and July in our model results which coincide with two observed marine heatwave events. At Darß Sill and Arkona Sea, these heating rate maxima were larger in May, by 0.18 and 0.35 K m^{-1}d^{-1}, respectively compared to July, while at Oder bank the heating rate maxima was larger in July by 0.1 K m^{-1}d^{-1}.

5 Conclusions

Heating rates due to absorption of short wave radiation (UV-VIS) in the Western Baltic Sea are controlled by the combined effects of the seasonal solar cycle and the concentration and distribution of OSCs. The intensity of radiative energy reaching the sea surface is locally modified by radiative transfer through the atmosphere, which is mostly controlled by cloudiness whose long term climatology minimum is observed in May (Dera and Woźniak, 2010). Further modulation of heating rates in the Western Baltic Sea in UV and VIS spectral domains is dependent on water transparency which is a complex function of the magnitude and seasonal cycles of inherent optical properties and the directionality of the light field. Our study found that in 2018 the combined effect of CDOM and particulate absorption on surface heating rates in the Western Baltic Sea could reach up to 0.4 to 0.8 K d^{-1}, during the productive period April to September, and is relevant from the surface down to 2-5 m depth. Moreover, this modelled OSC-induced surface warming results in a mean loss of heat (c. 5 Wm^{-2}) from the sea to the atmosphere, primarily in the form of latent and sensible heat fluxes, which may be significant for regional heat balance budgets. Two way coupling with the atmosphere is not included in our experiment, but we expect this would modulate (decrease) the magnitude of the net loss of heat to the atmosphere.

Anticipated and recently observed changes in phytoplankton functional types and their seasonal pattern and CDOM terrestrial input patterns due to global warming will further modulate the spatial and temporal pattern of heating rates in the Baltic Sea. Observed changes in the quantity and quality of CDOM, the composition and concentration of phytoplankton functional types and photosynthetic pigments and thus changes to the optical properties of the Baltic Sea, need to be communicated to coupled hydrodynamic-biogeochemical models such that the consequences of radiative feedbacks can be better understood and better predictions of the future Baltic Sea environment can be made. Further improvements to coupled hydrodynamic and ecological models are heavily dependent on the correct parameterization of the downwelling irradiance diffuse attenuation coefficient K_d, which requires a proper understanding of the seasonal

1023 and spatial variability of the optical properties in different water types. This work highlights the importance of K_d as a

1024 bio-optical driver: K_d provides a pathway to estimating heating rates and connects biological activity with energy fluxes.

1025

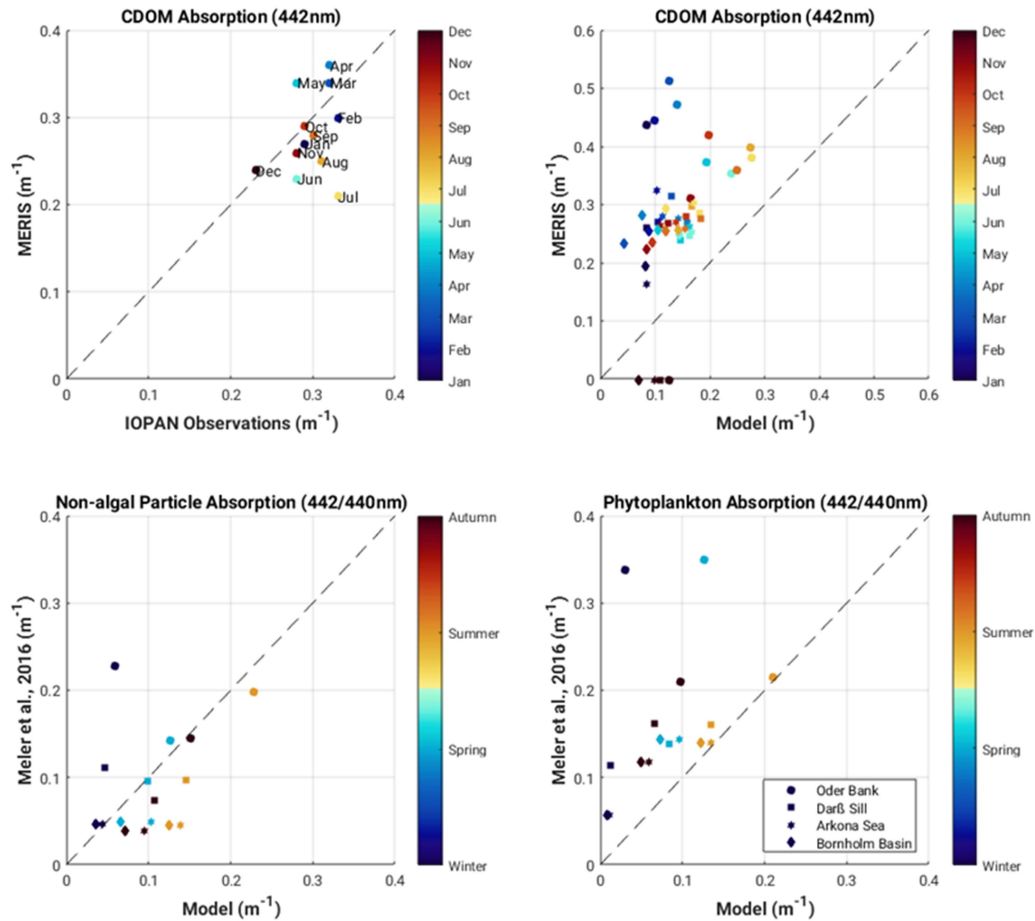1026 **Appendix A: Model versus in situ and remotely sensed observations**

1027

1028

1029 Figure A1: (a) MERIS and in situ monthly climatology of surface CDOM absorption (mean value calculated over
1030 Western Baltic Sea region shown in Figure 1); (b) mean monthly surface CDOM absorption at model stations and
1031 matching MERIS locations; seasonal mean surface non-algal particle absorption (CDOM+detritus) (c) and
1032 phytoplankton absorption (d) at model stations compared with similar water type values found in Meler et al. (2016).

1033

1034

Appendix A: Western Baltic Sea Model Setup

Table A1: Model configurations

ROMS Ecosim/BioOptic	
Application Name	3D Western Baltic Sea
Model Grid	285 x 169 (1.8km), 30 sigma levels
Simulation Period	2018
Boundary Conditions	Chapman for zeta, Flather for ubar and vbar; Radiation + Nudging for temperature and salinity
Bulk Flux Atmosphere	DWD-ICON 3-hourly
River Forcing	HELCOM PLC (Pollution Load Compilation), Neumann (pers. comm.)
Initial Conditions	GETM / ERGOM
Time Step	DT = 30s; NDTFAST = 20s
Ecosim	4 phytoplankton groups (small and large diatoms, large dinoflagellates & cyanobacteria)
Spectral Resolution	5 nm intervals between 400 and 700 nm
MOMO	
Angles	27 Atmosphere; 36 Ocean between 0 and 88 degrees
Layers	30 vertical ocean layers (depths equivalent to ROMS Ecosim/BioOptic)
Fourier Expansion	120 terms
Absorption & Scattering Coefficients	ROMS BioOptic Output
Spectral Resolution	5 nm intervals between 400 and 700 nm
Phase Function	Fournier and Forand, 1994; Freda and Piskozub, 2007 with differing backscattering to scattering ratios phytoplankton (bb/b = 0.001) and detrital material (bb/b = 0.1).

Appendix B: In situ and remotely sensed data used for climatologies

In situ measurements and remotely sensed data from the MERIS ocean colour archive of CDOM absorption at 443 nm were used to develop a climatologies of CDOM absorption which support the evaluation of our modelled estimates of CDOM absorption. Below, the source and processing of the different data sets are briefly described.

B1 In situ CDOM measurements and climatology

A time series (1994 - 2017) of in situ observations of CDOM absorption at 443 nm was reprocessed into seasonal means for our study area (Figure 1). This data set was collected as a result of the implementation of numerous research projects and statutory research programs conducted by the Remote Sensing Laboratory at the Institute of Oceanology, Polish Academy of Sciences (IOPAN), Sopot Poland in the whole Baltic Sea. The main aim of the study on CDOM optical properties was the assessment of its temporal and spatial variability (Kowalczuk and Kaczmarek, 1996, Kowalczuk, 1999) and its relation to hydrodynamic conditions and Baltic Sea productivity (Kowalczuk et al., 2006). As the primary goal of this research was the development and validation of ocean colour remote sensing algorithms (Kowalczuk et al., 2005a), the vast majority of samples for determination of CDOM absorption spectrum were collected in the surface layer. However, since 2014, samples were also collected within the water column, depending on the thermohaline stratification of water masses and depth distribution of autotrophic protists, in order to better resolve the impact of non-linear processes (i.e. photo-degradation, autochthonous production by phytoplankton, diffusion from bottom sediments) influencing CDOM optical properties (Kowalczuk et al., 2015). The sampling program is conducted in the whole Baltic Sea and is designed to resolve the spatial variability of the CDOM absorption coefficient. We use a subset of this time series located in our study area (Figure 1). Most of the samples were taken in spring and autumn, with a smaller number of samples collected in winter and summer mostly due to adverse weather conditions or unavailability of research vessels in summer months. Water samples were collected by Niskin bottle and were filtered first through acid-washed Whatman glass fibre filters (GF/F, nominal pore size 0.7 mm). The water was then passed through acid washed membrane filters with 0.2 mm pore to remove fine-sized particles. From 2014 until the present, water for CDOM absorption spectra were gravity filtered directly from Niskin bottles through Millipore Opticap XL4 Durapore filter cartridge with nominal pore size 0.2 μm. Filtered water was kept in acid washed amber glass 200 ml sample bottles until spectrophotometric analysis, which was performed with use of various models of bench top research grade, double beam spectrophotometers both in land base laboratory (Kowalczuk and Kaczmarek, 1996; Kowalczuk, 1999) and on the ship (Kowalczuk et al., 2005a,b, 2006). The cuvette pathlength was 5 or 10 cm depending on the spectrophotometer model. MilliQ water was used as the reference for all measurements. The absorption coefficient aCDOM(λ) was calculated as follows:

$$a_{CDOM}(\lambda) = \frac{2.303\,A(\lambda)}{L} \tag{B1}$$

where L is the optical path length, A is the absorptance (the flux that has been absorbed) and the factor 2.303 is the natural logarithm of 10.

The whole CDOM absorption data base in the IOPAN repository, collected between 1994 and 2017, was reprocessed to calculate the spectrum slope coefficient, S. A nonlinear least squares fitting method using a Trust-Region algorithm implemented in Matlab was applied (Stedmon et al., 2000, Kowalczuk et al., 2006) in the spectral range 300-600 nm, as follows:

$$a_{CDOM}(\lambda) = a_{CDOM}(\lambda_0)e^{-S(\lambda_0 - \lambda)} + K \tag{B2}$$

where λ_0 is 350 nm, and K is a background constant that allows for any baseline shift caused by residual scattering by fine size particle fractions, micro-air bubbles or colloidal material present in the sample, refractive index differences between sample and the reference, or attenuation not due to CDOM. The parameters aCDOM (350), S, and K were estimated simultaneously via non-linear regression using Eq. (12).

B2 Remotely sensed data

MERIS FRS L2 (full resolution level 2) product from 2003 to 2012 was used to create a monthly climatology of CDOM absorption for the Western Baltic Sea region. The MERIS FRS L2 product was processed with the C2RCC algorithm (Doerffer and Schiller, 2007) which has been trained with data-sets from European coastal waters. Full details of the post processing of the MERIS data into a climatology can be found in Röhrenbach (2019). A monthly climatology for the complete time frame of the MERIS archive was created and includes the mean value, standard deviation and number of observations for each point.

Figure A1 shows the difference between a snapshot of the MERIS data product (01.04.2004) and the corresponding April climatology. The snapshot has almost complete data coverage, which is quite rare compared to other time periods where only a small part of the region of interest is in the frame or free of cloud coverage. The climatology smooths the spatial variability, providing the average spatial distribution and gradients in CDOM absorption. High values of aCDOM(443) can be seen around the river mouths of the Vistula river (≈ 1.7 m^{-1}) and the Oder river (≈ 0.7 m^{-1}), whereas offshore areas show lower values (≈ 0.2 m^{-1}) and spatial variability. The snapshot image presents the typical situation at the beginning of the spring freshet. Both Vistula and Oder rivers have similar hydrographic properties with maximum flow observed in April and May and minimum flow in June and February. The land use in the catchment is also similar and consists of a mixture of agriculture, forestry and urbanised areas. The

difference in aCDOM(443) values and the spatial extent of fresh water plumes seen as areas with elevated CDOM absorption results from the geomorphology of the outlets. The Vistula River has artificial outlets, built in 1895, and this channel carries up to 90 % of the flow with only a small fraction feeding old deltaic branches, cut off by locks and dikes. The Oder river outlet is less transformed by human activity, and the Oder River feeds the Szczecin Lagoon which is connected to the coastal Baltic Sea via three inlets: two located in Poland (Swina and Dziwna) and one in Germany (Peene). The shallow Szczecin Lagoon acts as a buffer and biogeochemical reactor, where photochemical, microbial and physical (flocculation) transformation of CDOM may occur leading to effective decreased absorption values recorded on the marine side of the estuary.
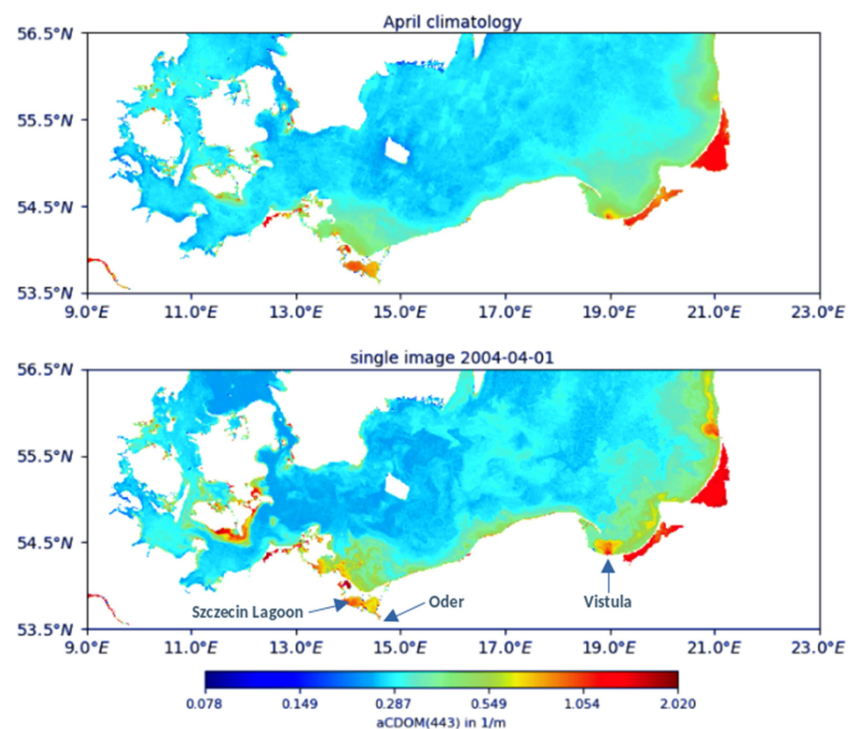
Figure B2.1: April climatology (top) and snapshot (01.04.2004) (bottom) of CDOM absorption at 443 nm (adapted from Röhrenbach, 2019).
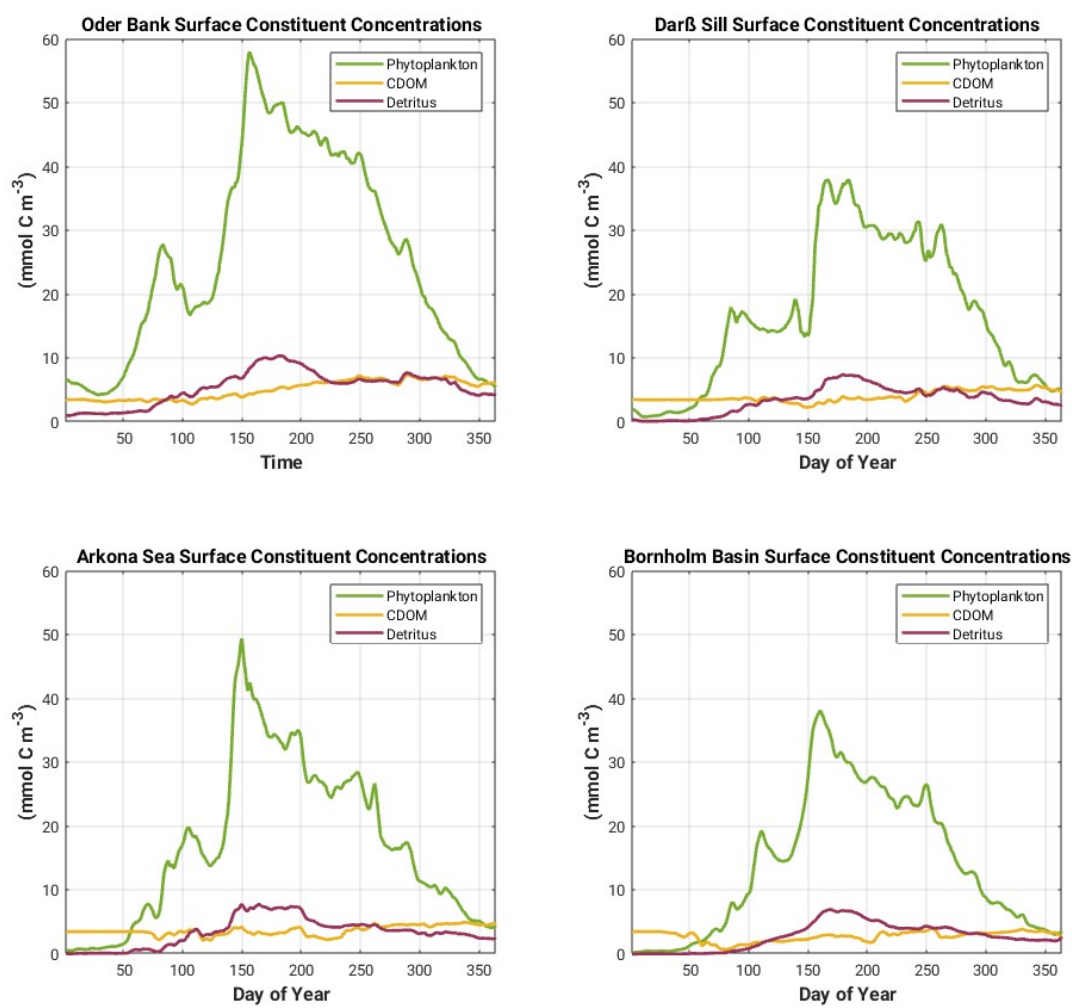
Appendix C: Modelled surface water constituent concentrations in 2018

1120 Figure C1: Modelled surface water constituent concentrations in 2018 at Oder Bank, Darß Sill, Arkona Sea and

1121 Bornholm Basin.

1122

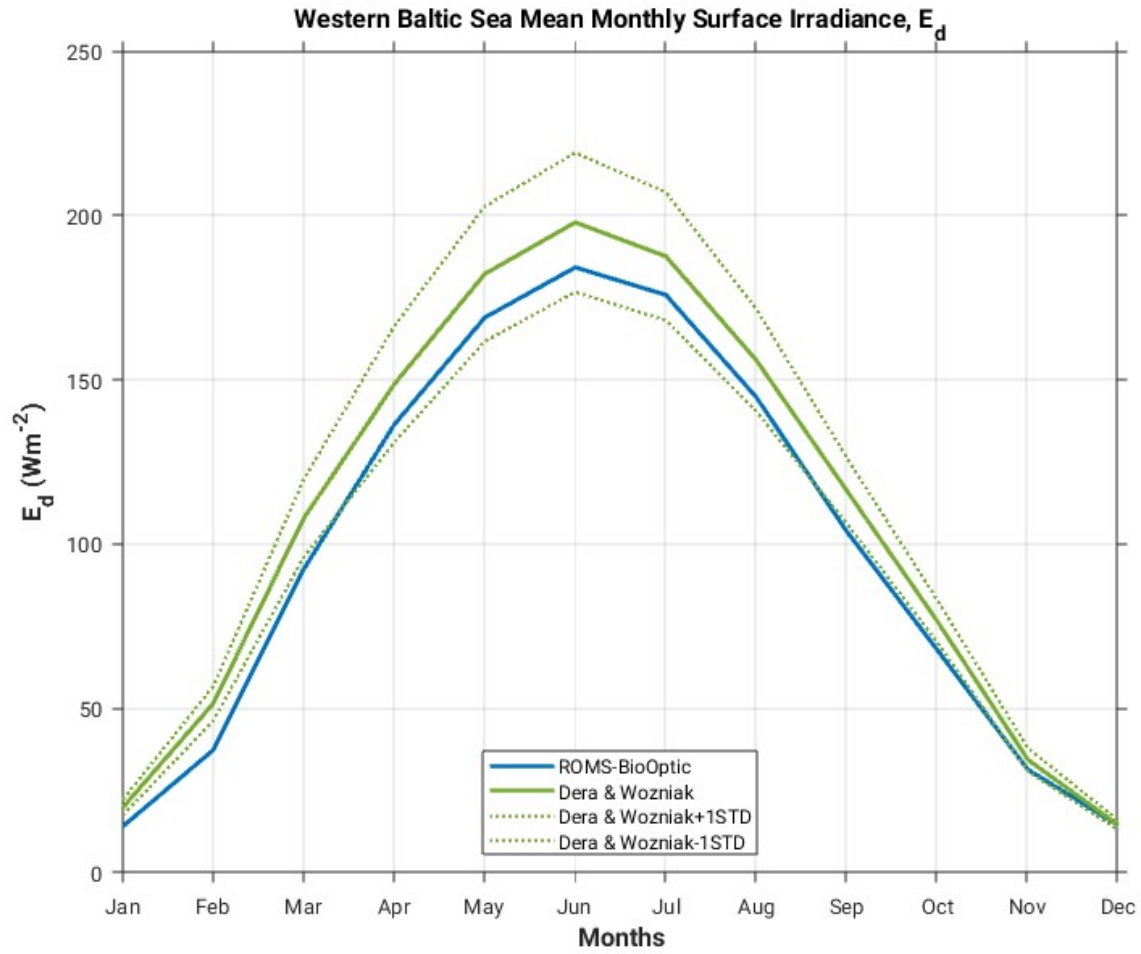1123   **Appendix D: Western Baltic Sea monthly mean surface irradiance**

1124

Western Baltic Sea Mean Monthly Surface Irradiance, E_d

1125

1126   Figure D1: Modelled monthly mean surface irradiance in the Western Baltic Sea, ROMS-BioOptic versus Dera &

1127   Wozniak, 2010 (Dashed green lines represent Dera & Wozniak +/- one standard deviation).

1128

1129

Code Availability:

The ROMS-Ecosim/BioOptic model code used in this study can be accessed at https:// www.myroms.org. The MOMO model code is available upon request from Jürgen Fischer, juergen.fischer@fu-berlin.de

Data availability:

The version of the Bio-Optic model code including the used to produce the resulbio_shortave feedbackts in this study, including and the initial conditions, river and boundary forcing are archived on Zenodo (10.5281/zenodo.7215110 reserved).

The atmospheric forcing data can be acquired for scientific research purposes upon request from Ulf Gräwe (ulf.graewe@io-warnemuende.de).

The MERIS FRS L2 CDOM absorption monthly climatology for the Western Baltic Sea used in this study is archived on Zenodo (10.5281/zenodo.775342510.5281/zenodo.7224656 - reserved).

The NOAA OI SST V2 High Resolution Dataset is available here: https://psl.noaa.gov/data/gridded/data.noaa.oisst.v2.highres.html

OLCI Level 3 300m Baltic Sea Ocean Colour Plankton, Transparency and Optics NRT daily observations were obtained from the Copernicus Marine Service, https://doi.org/10.48670/moi-00294.

The in situ CDOM absorption data can be acquired for scientific research purposes upon request from Piotr Kowalczuk (piotr@iopan.pl).

Author contributions:

BC conceived the study, extended the ECOSIM model code and set up the regional deployment of ROMS-BioOptic in the Western Baltic Sea. BC also performed all simulations and analysis, and wrote the manuscript with input from all co-authors. PK provided the in situ CDOM absorption data used in the study and made significant contributions to the manuscript. LK and JF provided support setting up the MOMO model code and expertise on radiative transfer theory in the ocean. UG provided model grid bathymetry, atmospheric forcing, as well as initial and boundary conditions. UG and JW provided support setting up and troubleshooting the regional deployment of ROMS in the Western Baltic Sea.

Competing interests:

The authors declare that they have no conflict of interest.

References

Aas, E.: Two-stream irradiance model for deep waters, Appl. Opt., 26, 2095 – 2101, https://doi.org/10.1364/AO.26.002095, 1987.

Ackleson, S., Balch, W. and Holligan, P.: Response of water-leaving radiance to particulate calcite and chlorophyll *a* concentrations: A model for Gulf of Maine coccolithophore blooms, Journal of Geophysical Research, 99(C4), https://doi.org/10.1029/93JC02150, 1994.

Alikas, K., Kratzer, S., Reinart, A., Kauer, T. and Paavel, B.: Robust remote sensing algorithms to derive the diffuse attenuation coefficient for lakes and coastal waters, Limnology and Oceanography: Methods, 13(8), 402 – 415, https://doi.org/10.1002/lom3.10033, 2015.

Alikas, K. and Kratzer, S.: Improved retrieval of Secchi depth for optically-complex waters using remote sensing data, Ecological Indicators, 77, 218 – 227, https:/doi.org/10.1016/J.ECOLIND.2017.02.007, 2017.

Belkin, I.: Rapid warming of large marine ecosystems, Progress in Oceanography, 81(1-4), 207 – 213, https://doi.org/10.1016/J.POCEAN.2009.04.011, 2009.

Bennartz, R. and Fischer, J.: A modified k-distribution approach applied to narrow band water vapour and oxygen absorption estimates in the near infrared, Journal of Quantitative Spectroscopy and Radiative Transfer, 539 – 553, https://doi.org/10.1016/S0022-4073(99)00184-3, 2000.

Bennartz, R. and Fischer, J.: Retrieval of columnar water vapour over land from backscattered solar radiation using the Medium Resolution Imaging Spectrometer, Remote Sensing of Environment, 78, 274 – 283, https://doi.org/10.1016/S0034-4257(01)00218-8, 2001.

Bidigare, R.R., Ondrusek, M.E., Morrow, J.H. and Kiefer, D.A.: In vivo absorption properties of algal pigments. P. SPIE, 1302, 290-302, doi:10.1117/12.21451, 1990.

Bissett, W., Walsh, J., Dieterle, D. and Carder, K.: Carbon cycling in the upper waters of the Sargasso Sea: I. Numerical simulation of differential carbon and nitrogen fluxes, Deep Sea Research Part I: Oceanographic Research Papers, 46(2), 205 – 269, https://doi.org/10.1016/S0967-0637(98)00062-4, 1999a.

Bissett, W., Walsh, J., Dieterle, D. and Carder, K.: Carbon cycling in the upper waters of the Sargasso Sea: II. Numerical simulation of apparent and inherent optical properties, Deep Sea Research Part I: Oceanographic Research Papers, 46(2), 271 – 317, https://doi.org/ 10.1016/S0967-0637(98)00063-6, 1999b.

Cahill, B., Schofield, O., Chant, R., Wilkin, J., Hunter, E., Glenn, S. and Bissett, P.: Dynamics of turbid buoyant plumes and the feedbacks on near-shore biogeochemistry and physics, Geophysical Research Letters, 35(19), 1 – 6, https://doi.org/.1029/2008GL033595, 2008.

Cahill, B., Wilkin, J., Fennel, K., Vandemark, D. and Friedrichs, M.: Interannual and seasonal variabilities in air-sea CO_2 fluxes along the U.S. eastern continental shelf and their sensitivity to increasing air temperatures and variable winds, Journal of Geophysical Research: Biogeosciences, 121(2), 295 – 311, https://doi.org/ 10.1002/2015JG002939, 2016.

Darecki, M., Weeks, A., Sagan, S., Kowalczuk, P. and Kaczmarek, S.: Optical characteristics of two contrasting Case 2 waters and their influence on remote sensing algorithms, Continental Shelf Research, 23(3-4), 237 – 250, https://doi.org/10.1016/S0278-4343(02)00222-4, 2003.

Darecki, M. and Stramski, D.: An evaluation of MODIS and SeaWiFS bio-optical algorithms in the Baltic Sea, Remote Sensing of Environment, 89(3), 326 – 350, https://doi.org/10.1016/J.RSE.2003.10.012, 2004.

Dera, J., and Woźniak, B.: Solar radiation in the Baltic Sea, Oceanologia, 52(4), 533–582, 2010.

Dickey, T. and Falkowski, P.: Solar energy and its biological-physical interactions in the sea, in *The Sea*, 12, eds. Allan R. Robinson, James J. McCarthy and Brian J. Rothschild, John Wiley & Sons, NY, ISBN 0-471-18901-4, 2002.

Doerffer, R. and Schiller, H.: The MERIS case 2 water algorithm, International Journal of Remote Sensing, 28(3-4), 517 – 535, https://doi.org/10.1080/01431160600821127, 2007.

Dutkiewicz, S., Hickman, A., Jahn, O., Gregg, W., Mouw, C. and Follows, M.: Capturing optically important constituents and properties in a marine biogeochemical and ecosystem model, Biogeosciences, 12(14), 4447 – 4481, https://doi.org/10.5194/bg-12-4447-2015, 2015.

Fasham, M. J. R.; Ducklow, H. W.; McKelvie, S. M.: A nitrogen-based model of plankton dynamics in the oceanic mixed layer, Journal of Marine Research, 48 (3), 591–639, doi:10.1357/002224090784984678, 1990.

Fell, F. and Fischer, J.: Numerical simulation of the light field in the atmosphere-ocean system using the matrix-operator method, Journal of Quantitative Spectroscopy and Radiative Transfer, 69(3), 351 – 388, https://doi.org/10.1016/S0022-4073(00)00089-3, 2001.

Fennel, K., Wilkin, J., Levin, J., Moisan, J., O'Reilly, J and Haidvogel, D.: Nitrogen cycling in the Middle Atlantic Bight: Results from a three dimensional model and implications for the North Atlantic nitrogen budget, Global Biogeochemical Cycles, 20(3), https://doi.org/10.1029/2005GB002456, 2006.

Fennel, K., Wilkin, J., Previdi, M. and Najjar, R.: Denitrification effects on air-sea CO_2 flux in the coastal ocean: Simulations for the northwest North Atlantic, Geophysical Research Letters, 35(24), https://doi.org/10.1029/2008GL036147, 2008.

Fennel, K. and Wilkin, J.: Quantifying biological carbon export for the northwest North Atlantic continental shelves, Geophysical Research Letters, 36(18), https://doi.org/10.1029/2009GL039818, 2009.

Fennel, K., Hu, J:, Laurent, A., Marta-Almeida, M and Hetland, R.: Sensitivity of hypoxia predictions for the northern Gulf of Mexico to seiment oxygen consumption and model nesting, Journal of Geophysical Research: Oceans, 118(2), 990 – 1002, https://doi.org/10.1002/jgrc.20077, 2013.

Fennel, W. and Sturm, M.: Dynamics of the western Baltic, Journal of Marine Systems, 3, 183-205, https://doi.org/10.1016/0924-7963(92)90038-A, 1992.

Fischer, J. and Grassl, H.: Radiative transfer in an atmosphere-ocean system: an azimuthally dependent matrix-operator approach, Applied Optics, 23(7), https://doi.org/10.1364/AO.23.001032, 1984.

Fournier, G.R. and Forand, J.L.: Analytic phase function for ocean water, Proc. SPIE 2258, Ocean Optics XII, https://doi.org/10.1117/12.190063, 1994.

Freda, W. and Piskozub, J.: Improved method of Fournier-Forand marine phase function parameterization, Optics Express, 15(20), 12763-12768, https://doi.org/10.1364/OE.15.012763, 2007.

Gallegos, C.L., Werdell, P.J and McClain, C.R.: Long-term changes in light scattering in Chesapeake Bay inferred from Secchi depth, light attenuation and remote sensing measurements, Journal of Geophysical Research, Oceans, 116, C7, https://doi.org/10.1029/2011JC007160, 2011.

Gnanadesikan, A., Kim, G. and Pradal, M.: Impact of colored dissolved materials on the annual cycle of sea surface temperature: potential implications for extreme ocean temperatures, Geophysical Research Letters, 46(2), 861 – 869, https://doi.org/10.1029/2018GL080695, 2019.

Goncalves-Araujo, R. and Markager, S.: Light in the dark: Retrieving underwater irradiance in shallow eutropic waters from AC-S measurements, Frontiers in Marine Science, 7, https://doi.org/ 10.3389/fmars.2020.00343, 2020.

Gordon, H.R., Smith, R.C. and Zaneveld, J.R.V.: Introduction to ocean optics, Proc. SPIE 0208, Ocean Optics VI., https://doi.org/10.1117/12.958262, 1980.

Gräwe, U., Holtermann, P., Klingbeil, K. and Burchard, H.: Advantages of vertically adaptive coordinates in numerical models of stratified shelf seas, Ocean Modelling, 92, 56 – 68, https://doi.org/10.1016/j.ocemod.2015.05.008, 2015a.

Gräwe, U., Naumann, M., Mohrholz, V and Burchard, H.: Anatomizing one of the largest saltwater inflows into the Baltic Sea in December 2014, Journal of Geophysical Research: Oceans, 120(11), 7676 – 7697, https://doi.org/10.1002/2015JC011269, 2015b.

Gregg, W.W.: A coupled ocean-atmosphere radiative model for global ocean biogeochemical model, NASA Technical Report Series on Global modelling and Data Assimilation, 22 (NASA/TM-2002-104606), 2002.

Guanter, L., Alonso, L., Gomez-Chova, L., Meroni, M., Preusker, R., Fischer, J and Moreno, J.: Developments for vegetation fluorescence retrieval from spaceborne high-resolution spectrometry in the O_{2-A} and O_{2-B} absorption bands, Journal of Geophysical Research, 115(D19), D19303, 10.1029/2009JD013716, 2010.

Gregg, W.W. and Carder, K.: A simple spectral solar irradiance model for cloudless maritime atmospheres, Limnology and Oceanography, 35(8), 1657 – 1675, https://doi.org/10.4319/lo.1990.35.8.1657, 1990.

Gregg, W.W. and Rousseaux, C.S.: Directional and spectral irradiance in ocean models: effects on simulated global phytoplankton, nutrients and primary production, Front. Mar. Sci., 22, 3, https://doi.org/10.3389/fmars.2016.00240, 2016.

Haidvogel, D., Arango, H., Budgell, W., Cornuelle, B., Curchitser, E., Lorenzo, E., Fennel, K., Geyer, W., Hermann, A., Lanerolle, L., Levin, J., McWilliams, J., Miller, J., Moore, A., Powell, T., Shchepetkin, A., Sherwood, C., Signell, R.,

Warner, J. and Wilkin, J.: Ocean forecasting in terrain-following coordinates: Formulation and skill assessment of the Regional Ocean Modeling System, Journal of Computational Physics, 227(7), 3595 3624, https://doi.org/10.1016/j.jcp.2007.06.016, 2008.

Heege, T. and Fischer, J.: Mapping of water constituents in Lake Constance using multispectral airborne scanner data and a physically based processing scheme, Canadian Journal of Remote Sensing, 30(1), 77 – 86, https://doi.org/10.5589/m03-056, 2004.

Hill, V.: Impacts of chromophoric dissolved organic material on surface ocean heating in the Chukchi Sea, Journal of Geophysical Research, 113(C7), C07024, https://doi.org/10.1029/2007JC004119, 2008.

Hollstein, A. and Fischer, J.: Radiative transfer solutions for coupled atmosphere ocean systems using the matrix operator technique, Journal of Quantitative Spectroscopy and Radiative Transfer, 113(7), 536 – 548, https://doi.org/10.1016/j.jqsrt.2012.01.010, 2012.

Huang, B., Liu, C., Banzon, V., Freeman, E., Graham, G., Hankins, B., Smith, T. and Zhang, H.-M.: Improvements of the Daily Optimum Interpolation Sea Surface Temperature (DOISST) Version 2.1, Journal of Climate, 34, 2923-2939. doi: 10.1175/JCLI-D-20-0166.1, 2021.

IPCC, 2019: Summary for Policymakers. In: IPCC Special Report on the Ocean and Cryosphere in a Changing Climate [H.-O. Pörtner, D.C. Roberts, V. Masson-Delmotte, P. Zhai, M. Tignor, E. Poloczanska, K. Mintenbeck, A. Alegría, M. Nicolai, A. Okem, J. Petzold, B. Rama, N.M. Weyer (eds.)]. Cambridge University Press, Cambridge, UK and New York, NY, USA, pp. 3–35. https://doi.org/10.1017/9781009157964.001.

IPCC, 2019: Summary for Policymakers. In: IPCC Special Report on the Ocean and Cryosphere in a Changing Climate [H.-O. Pörtner, D.C. Roberts, V. Masson-Delmotte, P. Zhai, M. Tignor, E. Poloczanska, K. Mintenbeck, A. Alegría, M. Nicolai, A. Okem, J. Petzold, B. Rama, N.M. Weyer (eds.)]. In press.

Isemer, H.J. and Rozwadowska, A.: Solar radiation fluxes at the surface of the Baltic Proper. Part 2. Uncertainties and comparison with simple bulk parameterization, Oceanologia, 41(2), 147-185, 1999.

Jerlov, N.G., Marine Optics, Elsevier, Amsterdam, 1976.

Jolliff, J. and Smith, T.: Biological modulation of upper ocean physics: Simulating the biothermal feedback effect in Monterey Bay, California, Journal of Geophysical Research: Biogeosciences, 119(5), 703 – 721, https://doi.org/10.1002/2013JG002522, 2014.

Karhu, M., Elmgren, R. and Savchuk, O.: Changing seasonality of the Baltic Sea, Biogeosciences, 13(4), 1009 – 1018, https://doi.org/10.5194/bg-13-1009-2016, 2016.

Kim, G., Pradal, M. and Gnanadesikan, A.: Quantifying the biological impact of surface ocean light attenuation by colored detrital matter in an ESM using a new optical parameterization, Biogeosciences, 12(16), 5199 – 5132, https://doi.org/10.5194/bg-12-5119-2015, 2015.

Kim, G., Gnanadesikan, A. and Pradal, M.: Increased surface ocean heating by colored detrital matter (CDM) linked to greater northern hemisphere ice formation in the GFDL CM2Mc ESM, Journal of Climate, 29(24), 9063 – 9076, https://doi.org/ 10.1175/JCLI-D-16-0053.1, 2016.

Kim, G., Gnanadesikan, A. Del Castillo, C. and Pradal, M.: Upper ocean cooling in a coupled climate model due to light attenuation by yellowing materials, Geophysical Research Letters, 45(12), 6134 – 6140, https://doi.org/10.1029/2018GL077297, 2018.

Kim, G., St-Laurent, P., Friedrichs, M. and Mannino, A.: Impacts of water clarity variability on temperature and biogeochemistry in the Chesapeake Bay, Estuaries and Coasts, 43(8) 1973 – 1991, https://doi.org/10.1007/s12237-020-00760-x, 2020.

Kirk, J.T.O.: Light and Photosynthesis in Aquatic Systems, 3rd Edition, University Press, Cambridge, 649pp, 2011.

Kowalczuk, P.: Seasonal variability of yellow substance absorption in the surface layer of the Baltic Sea, Journal of Geophysical Research - Oceans, 104(C12), 30 047-30 058, 1999.

Kowalczuk, P. And Kaczmarek, S.: Analysis of temporal and spatial variability of "yellow substance" absorption in the Southern Baltic, Oceanologia, 38(1), 3-32, 1996.

Kowalczuk, P., Sagan, S., Olszewski, J., Darecki, M. and Hapter,R.: Seasonal changes in selected optical parameters in the Pomeranian Bay in 1996-1997, Oceanologia, 41(3), 309-334, 1999.

Kowalczuk, P., Olszewski, J., Darecki, M. and Kaczmarek, S.: Empirical relationships between Coloured Dissolved Organic Matter (CDOM) absorption and apparent optical properties in Baltic Sea waters, International Journal of Remote Sensing, 26(2), 345-370, 2005a.

Kowalczuk, P., Stoń-Egiert, J., Cooper, W.–J., Whitehead, R.–F. And and Durako, M.–J.: Characterization of Chromophoric Dissolved Organic Matter (CDOM) in the Baltic Sea by Excitation Emission Matrix fluorescence spectroscopy. Marine Chemistry, 96, 273-292, 2005b.

Kowalczuk P., Stedmon, C.–A. and Markager, S.: Modelling absorption by CDOM in the Baltic Sea from season, salinity and chlorophyll, Marine Chemistry, 101, 1-11, 2006.

Kowalczuk, P., Sagan, S., Zablocka, M. and Borzycka, K.: Mixing anomaly in deoxygenated Baltic Sea deeps indicates benthic flux and microbial transformation of chromophoric and fluorescent dissolved organic matter, Estuarine, Coastal and Shelf Science, 163, 206 – 217, https://doi.org/10.1016/j.ecss.2015.06.027, 2015.

Kratzer, S., Hakansson, B. and Sahlin, C.: Assessing Secchi and photic zone depth in the Baltic sea from satellite data, Ambio, 32(8), 577 – 585, https://www.jstor.org/stable/4315443, 2003.

Kratzer, S. and Moore, G.: Inherent optical properties of the Baltic Sea in comparison to other seas and oceans, Remote Sensing, 10(3), https://doi.org/10.3390/rs10030418, 2018.

Kritten, L., Preusker, R. and Fischer, J.: A new retrieval of sun-induced chlorophyll fluorescence in water from ocean colour measurements applied on OLCI L-1b and L-2, Remote Sensing, 12(23), 1 – 24, https://doi.org/10.3390/rs12233949, 2020.

Lee, Z., Du, K. and Arnone, R.: A model for the diffuse attenuation coefficient of downwelling, Journal of Geophysical Research: Oceans, 110(2) 1 – 10, https://doi.org/10.1029/2004JC002275, 2005.

Lewis, M., Carr, M., Feldman, G., Esaias, W. and McClain, C.: Influence of penetrating solar radiation on the heat budget of the equatorial Pacific Ocean, Nature, 347, https:/doi.org/https://doi.org/10.1038/347543a0, 1990.

Lindstrot, R., Preusker, R. and Fischer, J.: The retrieval of land surface pressure from MERIS measurements in the oxygen a band, Journal of Atmospheric and Oceanic Technology, 26(7), 1367 – 1377, https://doi.org/10.1175/2009JTECHA1212.1, 2009.

Löptien, U. and Meier, H.E.M.: The influence of increasing water turbidity on the sea surface temperature in the Baltic sea: A model sensitivity study, Journal of Marine Systems, 88(2), 323 – 331, https://doi.org/10.1016/J.JMARSYS.2011.06.001, 2011.

Lund-Hansen, L.: Diffuse attenuation coefficients K_d(PAR) at the estuarine North Sea-Baltic Sea transition: time-series, partitioning, absorption and scattering, Estuarine, Coastal and Shelf Science, 61(2), 251 – 259, https://doi.org/10.1016/J.ECSS.2004.05.004, 2004.

Łysiak-Pastuszak, E., Drgas, N. and Piatkowska, Z.: Eutrophication in the Polish coastal zone: the past, present status and future scenarios, Mar. Pollut. Bull. 49 (3), 186–195, https://doi.org/10.1016/j.marpolbul.2004.02.007, 2004.

Manizza, M., Quere, C., Watson, A. and Buitenhuis, E.: Bio-optical feedbacks among phytoplankton, upper ocean physics and sea-ice in a global model, Geophysical Research Letters, 32(5), 1 – 4, https://doi.org/10.1029/2004GL020778, 2005.

Manizza, M., Quere, C., Watson, A. and Buitenhuis, E.: Ocean biogeochemical response to phytoplankton-light feedback in a global model, Journal of Geophysical Research: Oceans, 113(10), https://doi.org/10.1029/2007JC004478, 2008.

Meier, H.E.M.: Modeling the pathways and ages of inflowing salt- and freshwater in the Baltic Sea, Estuarine Coastal Shelf Science, 74(4), 717-734, https://doi.org/10.1016/j.ecss.2007.05.019, 2007.

Meier, H. E. M., Kniebusch, M., Dieterich, C., Gröger, M., Zorita, E., Elmgren, R., Myrberg, K., Ahola, M. P., Bartosova, A., Bonsdorff, E., Börgel, F., Capell, R., Carlén, I., Carlund, T., Carstensen, J., Christensen, O. B., Dierschke, V., Frauen, C., Frederiksen, M., Gaget, E., Galatius, A., Haapala, J. J., Halkka, A., Hugelius, G., Hünicke, B., Jaagus, J., Jüssi, M., Käyhkö, J., Kirchner, N., Kjellström, E., Kulinski, K., Lehmann, A., Lindström, G., May, W., Miller, P. A., Mohrholz, V., Müller-Karulis, B., Pavón-Jordán, D., Quante, M., Reckermann, M., Rutgersson, A., Savchuk, O. P., Stendel, M., Tuomi, L., Viitasalo, M., Weisse, R., and Zhang, W.: Climate change in the Baltic Sea region: a summary, Earth Syst. Dynam., 13, 457–593, https://doi.org/10.5194/esd-13-457-2022, 2022.

Meler, J., Ostrowska, M., Stoń-Egiert, J. and Zabłocka., M.: Seasonal and spatial variability of light absorption by suspended particles in the southern Baltic: A mathematical description, Journal of Marine Systems, 170, 68 – 87, https://doi.org/10.1016/J.JMARSYS.2016.10.011, 2017.

Meler, J., Ostrowska, M. and Stoń-Egiert, J.: Seasonal and spatial variability of phytoplankton and non-algal absorption in the surface layer of the Baltic, Estuarine, Coastal and Shelf Science, 180, 123 – 135, https://doi.org/10.1016/J.ECSS.2016.06.012, 2016a.

Meler, J., Kowalczuk, P., Ostrowska, M., Zabłocka, M. and Zdun, A.: Parameterization of the light absorption properties of chromophoric dissolved organic matter in the Baltic Sea and Pomeranian lakes, Ocean Science, 12(4), 1013 – 1032, https://doi.org/ 10.5194/os-12-1013-2016, 2016b.

Morel, A. and Prieur, L.: Analysis of variations in ocean color, Limnology and Oceanography, 2(4), 709 – 722, https://doi.org/10.4319/lo.1977.22.4.0709, 1977.

Morel, A.: Optical modelling of the upper ocean in relation to its biogenous matter content (Case I waters), Journal of Geophysical Research, 93, 749 – 768, https://doi.org/10.1029/JC093iC09p10749, 1988.

Morel, A. and Antoine, D.: Heating rate within the upper ocean in relation to its bio-optical state, Journal of Physical Oceanography, 24, 1652 – 1665, https://doi.org/10.1175/1520-0485(1994)024%3C1652:HRWTUO%3E2.0.CO;2, 1994.

Murtugudde, R., Beauchamp, J., McClain, C., Lewis, M. and Busalacchi, A.: Effects of penetrative radiation on the upper tropical ocean circulation, Journal of Climate, 15, 470 – 486, https://doi.org/10.1175/1520-0442(2002)015%3C0470:EOPROT%3E2.0.CO;2, 2002

Neumann, T., Siegel, H. and Gerth, M.: A new radiation model for Baltic Sea ecosystem modelling, Journal of Marine Science, 152, 83 – 91, https://doi.org/10.1016/j.jmarsys.2015.08.001, 2015.

Neumann, T., Koponen, S., Attila, J., Brockmann, C., Kallio, K., Kervinen, M., Mazeran, C., Müller, D., Philipson, P., Thulin, S., Väkevä. S. and Ylöstalo, P.: Optical model for the Baltic Sea with an explicit CDOM state variable: A case study with Model ERGOM (version 1.2), Geoscientific Model Development, 14(8), 5049 – 5062, https://doi.org/10.5194/gmd-14-5049-2021, 2021.

Ohlmann, J., Siegel, D. and Gautier, C.: Ocean mixed layer radiant heating and solar penetration: A global analysis, Journal of Climate, 9, https://doi.org/10.1175/1520-0442(1996)009%3C2265:OMLRHA%3E2.0.CO;2, 1996.

Ohlmann, J., Siegel, D. and Washburn, L.: Radiant heating of the western equatorial Pacific during TOGA-COARE, Journal of Geophysical Research: Oceans, 103(C3), 5379 – 5395, https://doi.org/ 10.1029/97jc03422, 1998.

Ohlmann, J., Siegel, D. and Mobley, C.: Ocean radiant heating. Part I: Optical Influences, Journal of Physical Oceanography, 30, 1833 – 1848, https://doi.org/10.1175/1520-0485(2000)030%3C1833:ORHPIO%3E2.0.CO;2, 2000.

Ohlmann, J. and Siegel, D.: Ocean radiant heating. Part II: Parameterizing solar radiation transmission through the upper ocean, Journal of Physical Oceanography, 30, 1833 – 1848, https://doi.org/10.1175/1520-0485(2000)030%3C1849:ORHPIP%3E2.0.CO;2, 2000.

Omstedt, A. and Nohr, C.: Calculating the water and heat balances of the Baltic Sea using ocean modelling and available meteorological, hydrological and ocean data, Tellus A: Dynamic Meteorology and Oceanography, 56(4), 400 – 414, https://doi.org/10.3402/tellusa.v56i4.14428, 2004.

Omstedt, A., Pettersen, C., Rodhe, J. and Winsor, P.: Baltic Sea climate: 200 yr of data on air temperature, sea level variation, ice cover, and atmospheric circulation, Clim. Res., 25(3), 205–216, https://www.jstor.org/stable/24868400, 2004.

Oschlies, A.: Feedbacks of biotically induced radiative heating on upper-ocean heat budget, circulation and biological production in a coupled ecosystem-circulation model, Journal of Geophysical Research: Oceans, 109(12), 1 – 12, https://doi.org/10.1029/2004JC002430, 2004.

Paulson, C and Simpson, J.: Irradiance measurements in the upper ocean, Journal of Physical Oceanography, 7, 952 – 956, https://doi.org/10.1175/1520-0485(1977)007%3C0952:IMITUO%3E2.0.CO;2, 1977.

Pefanis, V., Losa, S. N., Losch, M., Janout, M. A. and Bracher, A: Amplified Arctic surface warming and sea ice loss due to phytoplankton and colored dissolved material, Geophysical Research Letters, 47, e2020GL088795, https://doi.org/10.1029/2020GL088795 , 2020.

1416 Röhrenbach, J.: Seasonal variability in the absorption of coloured dissolved organic matter (CDOM) in the western and
1417   southern Baltic Sea, Bachelor Thesis, Department of Earth Sciences, Free University Berlin, November 2019.

1418 Rozwadowska, A. and Isemer, H.J.: Solar irradiation fluxes at the surface of the Baltic Proper. Part 1. Mean annual
1419   cycle and influencing factors, Oceanologia, 40(4), 307-330, 1998.

1420 Sathyendranath, S. and Platt, T.: The spectral irradiance field at the surface and in the interior of the ocean: A model for
1421   applications in oceanography and remote sensing, Journal of Geophysical Research, 93(C8),
1422   https://doi.org/10.1029/JC093iC08p09270, 1988.

1423 Sathyendranath, S., Prieur, L and Morel, A.: A three-component model of ocean colour and its application to remote
1424   sensing of phytoplankton pigments in coastal waters, International Journal of Remote Sensing, 10(8) 1373 – 1394,
1425   https://doi.org/ 10.1080/01431168908903974, 1989.

1426 Shchepetkin, A. and McWilliams, J.: The regional oceanic modelling system (ROMS): A split-explicit, free-surface,
1427   topography-following-coordinate ocean model, Ocean Modelling, 9(4), 347 – 404,
1428   https://doi.org/10.1016/j.ocemod.2004.08.002, 2005.

1429 Siegel, H., Gerth, M., Ohde, T. and Heene, T.: Ocean colour remote sensing relevant water constituents and optical
1430   properties of the Baltic Sea, International Journal of Remote Sensing, 26(2), 315 – 330,
1431   https://doi.org/10.1080/01431160410001723709, 2005.

1432 Simis, S., Ylöstalo, P., Kallio, K., Spilling, K. and Kutser, T.: Contrasting seasonality in optical biogeochemical
1433   properties of the Baltic Sea, PLOS ONE, 12(4), https://doi.org/10.1371/journal.pone.0173357, 2017.

1434 Simpson, J. and Dickey, T.: Alternative parameterizations of downward irradiance and their dynamical significance,
1435   Journal of Physical Oceanography, 11, 876 – 882,
1436   https://doi.org/10.1175/1520-0485(1981)011%3C0876:APODIA%3E2.0.CO;2, 1981.

1437 Skákala, J., Bruggeman, J., Ford, D., Wakelin, S., Akpınar, A., Hull, T., Kaiser, J., Loveday, B.R., O'Dea, E., Williams,
1438   C.A.J. and Ciavatta, S.: The impact of ocean biogeochemistry on physics and its consequences for modelling shelf
1439   seas, Ocean Modelling, 172, https://doi.org/10.1016/j.ocemod.2022.101976, 2022.

1440 Soppa, A., Pefanis, V., Hellmann, S., Losa, S., Hölemann J., Janout, M., Martynov, F., Heim, B., Dinter, R., Rozanov, V.
1441   and Bracher, A.: Assessing the influence of water consitutents on the radiative heating of Laptev Sea shelf waters,
1442   Frontiers in Marine Science, https://doi.org/10.3389/fmars.2019.00221, 2019.

1443 Stedmon, C., Markager, S. and Kaas, H.: Optical properties and signatures of chromophoric dissolved organic matter
1444   (CDOM) in Danish coastal waters, Estuarine, Coastal and Shelf Science, 51(2), 267 – 278,
1445   https://doi.org/10.1006/ecss.2000.0645, 2000.

1446 Stoń-Egiert, J. and Ostrowska, M.: Long-term changes in phytoplankton pigment contents in the Baltic Sea: Trends and
1447   spatial variability during 20 years of investigations, Continental Shelf Research 236 (2022) 104666,
1448   doi:10.1016/j.csr.2022.104666, 2022.

1449 Taucher, J. and Oschlies, A.: Can we predict the direction of marine primary production change under global warming?
1450   Geophysical Research Letters, 38(2), https://doi.org/10.1029/2010GL045934, 2011.

1451 Terzic, E., Lazzari, P., Organelli, E., Solidoro, C., Salon, S., D'Ortenzio, F. and Conan, P.: Merging bio-optical data
1452   from Biogeochemical-Argo floats and models in marine biogeochemistry, Biogeosciences, 16(12), 2527 – 2542,
1453   https://doi.org/10.1029/2021JC017690, 2019.

1454 Terzic, E., Miro, A., Organelli, E., Kowalczuk, P., D'Ortenzio, F and Lazzari, P.: Radiative transfer modelling with
1455   Biogeochemical –Argo float data in the Mediterranean Sea, Journal of Geophysical Research: Oceans, 126(10),
1456   https://doi.org/10.1029/2021JC017690, 2021a.

1457 Terzic, E., Salon, S., Cossarini, G., Solidoro, C., Teruzzi, A., Miro, A. and Lazzari, P.: Impact of interannually variable
1458   diffuse attenuation coefficients for downwelling irradiance on biogeochemical modelling, Ocean Modelling, 161,
1459   https://doi.org/10.1016/J.OCEMOD.2021.101793, 2021b.Wetzel, P., Maier-Reimer, E., Botzet, M., Jungclaus, J.,
1460 Keenlyside, N. and Latif, M.: Effects of ocean biology on the penetrative radiation in a coupled climate model, Journal
1461   of Climate, 19, 3973 – 3987, https://doi.org/10.1175/JCLI3828.1, 2006.

1462 Wilkin, J., Zhang, W. G., Cahill, B. and Chant, R. C.: Integrating coastal models and observations for studies of ocean
1463   dynamics, observing systems and forecasting, In Operational Oceanography in the 21st Century, A. Schiller and G.
1464   Brassington (Eds.), Springer, doi: 10.1007/978-94-007-0332-2_19, 2011.

Wohlers, J., Engel, A., Breithaupt, P., Jü, K., Hoppe, H., Sommer, U. and Riebesell, U.: Changes in biogenic carbon flow in response to sea surface warming, PNAS, 106 (17) 7067-7072, https://doi.org/10.1073/pnas.0812743106, 2009.

Zaneveld, J. and Spinrad, R.: An arc tangent model of irradiance in the sea, Journal of Geophysical Research, 85(C9), https://doi.org/ 10.1029/JC085iC09p04919, 1980.

Zängl, G., Reinert, D., Rípodas, P. and Baldauf, M: The ICON (ICOsahedral Non-hydrostatic) modelling framework of DWD and MPI-M: Description of the non-hydrostatic dynamical core, Quarterly Journal of the Royal Meteorological Society, 141(687), 563–579, https://doi.org/10.1002/qj.2378, 2015.

Zdun, A., Stoń -Egiert, J., Ficek, D and Ostrowska, M.: Seasonal and Spatial Changes of Primary Production in the Baltic Sea (Europe) Based on in situ Measurements in the Period of 1993–2018, Front. Mar. Sci. 7:604532., doi: 10.3389/fmars.2020.604532, 2021.

Zhang, T., Fell, F., Zhi-Shen, L., Preusker, R., Fischer, J. and Ming.Xia, H.: Evaluating the performance of artificial neural network techniques for pigment retrieval from ocean color in Case I waters, Journal of Geophysical Research, 108(C9), https://doi.org/10.1029/2002JC001638, 2003.

Zielinski, O., Llinas, O., Oschlies, A. and Reuter, R.: Underwater light field and its effect on a one-dimensional ecosystem model at station ESTOC, north of the Canary Islands, Deep Sea Research II; 49, 17, https://doi.org/10.1016/S0967-0645(02)00096-6, 2002.